NOTICE

The quality of this microform is heavily dependent upon the quality of the original thesis submitted for microfilming. Every effort has been made to ensure the highest quality of reproduction possible.

If pages are missing, contact the university which granted the degree.

Some pages may have indistinct print especially if the original pages were typed with a poor typewriter ribbon or if the university sent us an inferior photocopy.

Reproduction in full or in part of this microform is governed by the Canadian Copyright Act, R.S.C. 1970, c. C-30, and subsequent amendments.

AVIS

La qualité de cette microforme dépend grandement de la qualité de la thèse soumise au microfilmage. Nous avons tout fait pour assurer une qualité supérieure de reproduction.

S'il manque des pages, veuillez communiquer avec l'université qui a conféré le grade.

La qualité d'impression de certaines pages peut laisser à désirer, surtout si les pages originales ont été dactylographiées à l'aide d'un ruban usé ou si l'université nous a fait parvenir une photocopie de qualité inférieure.

La reproduction, même partielle, de cette microforme est soumise à la Loi canadienne sur le droit d'auteur, SRC 1970, c. C-30, et ses amendements subséquents.

ISBN 0-315-53278-5

Context-dependent enhancements for digitized chest radiographs

by

Brigitte Plessis

A THESIS
submitted to the School of Graduate Studies and Research
in partial fulfillment of the requirements
for the degree of
MASTER OF APPLIED SCIENCE
in
Electrical Engineering

Ottawa-Carleton Institute for Electrical Engineering
Department of Electrical Engineering
Faculty of Engineering
University of Ottawa

August, 1989

Il faut pourtant saisir l'utopie, lui imposer le joug du réel et l'encadrer dans le fait. L'idée abstraite doit se transformer en idée concrète; ce qu'elle perd en beauté, elle le regagne en utilité; elle est moindre mais meilleure.

Quatre-vingt-treize, Victor Hugo.

Abstract

For the digitized radiograph to be widely accepted by the medical community, they must at least equal the quality of conventional radiographs and if possible exceed it. The object of this thesis is to investigate methods for improving the quality of the perceived digitized radiograph. The approach is to propose different enhancements at different phases of the reading process:

1. global enhancements for the "gestalt" view,
2. adaptive global enhancements for focussing on specific large anatomical features,
3. local enhancements for scrutiny on localized pathological features.

This work concentrates on chest radiographs as these are the most difficult to image. Results of user evaluation trials on the appearance of enhanced images are presented for the three phases of the reading process and allow to identify potentially useful transformations.

A new context-dependent technique is also proposed and called *Parametric Histogram Specification*. It consists in matching the histogram of a given poor quality image to that of an image which has been rated of good quality without altering the anatomical and pathological characteristics of the poor quality image.

Remerciements

Les deux années qui m'ont conduite à l'achèvement de ce Master ont été très enrichissantes. J'y ai mûri et appris et ce, essentiellement, grâce à mon superviseur Dr. Morris Goldberg. Je lui suis extrêmement reconnaissante pour son soutien, son dynamisme, sa perspicacité et ses conseils éclairés.

J'aimerais aussi remercier Dr. Dillon, Dr. Tombaugh, Marjorie Coristine et Cynthia Houston pour leur assistance dans la préparation des tests à l'hôpital.

Des remerciements très particuliers vont à Christian Robert pour son constant soutien et ses suggestions en Statistique.

Je remercie le Ministère des Affaires Etrangères du Gouvernement canadien et particulièrement les responsables de mon programme de bourses au sein de l'EUMC, pour leur soutien financier et amical.

Je garde un formidable souvenir de mon passage à l'Université d'Ottawa grâce à tous les membres du projet MUSIC et à tous mes amis étudiants. Je les en remercie sincèrement.

Contents

List of Figures

List of Tables

Chapter 1

Introduction

The use of digitized radiographs has been stimulated by the advent of Picture Archiving and Communication Systems (PACS) in hospitals [HEDGE, 86], [NOSIL, 88]. PACS acquire digital images store them as part of a multimedia file, transmit them to remote areas and present them on Cathode Ray Tubes (CRT).

For digitized radiographs to be widely accepted by the medical community, they must be of diagnostic quality. This implies that their quality needs to be at least equal the quality of conventional radiographs and if possible to exceed it. This is particularly essential in the case of chest radiographs which are the most frequent images in radiology and which are also difficult to image optimally because of the complexity of the human chest [JOHNSON, 85]. It is implicit that if digitized chest radiographs are accepted by radiologists and physicians, presumably along with necessary digital manipulations, digitized radiographs which image any other part of the body will also be accepted, and the manipulations for an acceptable digital representation will be derived easily.

In evaluating the quality of a digitized chest radiograph, two important parameters are the spatial resolution and the contrast resolution. Spatial resolution is related to the ability to discriminate fine details in the field of view. Contrast resolution refers to the smallest noticeable difference in luminance between a small object and its background. The jury is still out on the minimum spatial resolution required for diagnostic quality. The

results given in the literature range from 1000 to 4000 for a standard chest radiograph with 10 to 12 bits for contrast. An important practical consideration is the cost and availability of technology which at present implies the use of displays with 1000 lines of resolution and 8 bits of contrast. However, these technical limitations can be overcome by the potential for digital imaging systems to manipulate image data. In particular, the diagnostic value of digitized chest radiographs can be improved by applying various techniques which can enhance the overall picture appearance and which can bring out diagnostically relevant features.

Many techniques have been proposed to enhance digitized chest radiographs. The first class of enhancements proposed in the literature include spatial smoothing, grey-scale transformations and edge enhancement [COCKLIN, 83]. We refer to these techniques as *context-free* as the same process is performed to each pixel in the image independently of the spatial coordinates. Because they do not adapt to the local context on the image, their results are often disappointing [MCADAMS, 86]. Some alternatives are enhancement techniques where the transformations vary depending upon the local statistics in the image. We refer to these techniques as *context-sensitive*, examples are *Regionally adaptive histogram equalization* [SHERRIER, 87] and *Adaptive filtration* [MCADAMS, 87]. In the former technique, histograms are calculated locally and then modified according to statistical values of that region. In the latter technique, the histogram of the image is used to determine the regions in which an adapted edge enhancement operator is applied.

As image enhancement involves the improvement of visual quality, some form of subjective evaluation is often necessary. For this purpose, the radiologists and the physicians are the best judges. One further consideration is the amount and degree of user control required in the image enhancement process. The end goal would be a system capable of responding automatically to the viewing requirements of radiologists and physicians.

Our research work is oriented towards automatic context-dependent enhancements.

The object of this thesis is to understand the viewing requirements involved in the review of a chest radiograph and to determine the relevance of various enhancement techniques to meet these requirements.

Our work is based on the three-phase procedure involved in viewing a radiograph: (1) getting a global impression, (2) analysing the objects and the local features, and (3) focussing attention on local image perturbations. To support these three different phases, we propose three different type of enhancement procedures. The role of the first is to yield an appropriate compromise or baseline image matched to the "gestalt" requirement. The second enhancement is then invoked to aid in the analysis of local features. Finally local enhancements are used to highlight local image perturbations. The relevance of these enhancements is determined by subjective evaluation tests.

According to some results of these tests, we propose a new enhancement technique, called *Parametric Histogram Specification*, which automatically improves the appearance of "poor" quality images. Its basis first relies on the definition of a parametric model characterizing the histogram of digitized chest radiographs. Then it specifies the final parametrized model by combining some parameters of "good" quality chest images with inherent parameters of the "poor" quality image.

This work was carried out in the context of the MUSIC (MUltimedia System for Integrated Communications) project , a multi-disciplinary (network, multimedia, database, image processing, user interface) research effort of the University of Ottawa Medical Communications Centre.

The thesis is organized as follows. We first briefly present in Chapter 2 both the analog and digital characteristics of chest radiography. In chapter 3, we review the enhancement techniques which have been proposed in particular for chest images. Then, in chapter 4, we report on subjective evaluation trials for global enhancements and global adaptive enhancements to support the two first phases involved in viewing a radiograph, as well as

on the applicability of various grey-level reversal transformations. This follows in chapter 5 with the report of subjective evaluation tests on local enhancements for the third phase of the reviewing procedure. The new *Parametric Histogram Specification* technique is presented in chapter 6. Finally, in chapter 7, we summarize the results of this work and provide some suggestions for further investigations.

Chapter 2

Analog versus digital radiography: case of the chest

2.1 Introduction

Radiographic examination of the chest are the most commonly performed examination in hospitals. Nonetheless the challenges in attempting to image the chest are among the greatest encountered in trying to image any part of the body. The major challenge in producing a good chest radiograph is that an extremely wide range of information reaches the image receptor.

Digital radiography arouses interest and research efforts which are motivated by the development of PACS. It definitely has potential advantages to circumvert the problems of producing a good chest radiograph.

In this chapter, we present the analog and digital radiographic modalities in the case of the chest. After a brief insight on digital imaging in medicine, we report on chest imaging and reviewing. We then give a short overview of conventional chest radiography, followed by an introduction to digital chest radiography. As an example, we present the digital radiographic system which has been used for this thesis. Finally, we propose a three-phase enhancement task for digital chest radiograph reviewing.

2.2 Digital imaging in medicine

The radiograph was the first imaging modality to be introduced in medicine at the end of the last century and it is still the most commonly used nowadays. In the 1970's, computed tomography (CT) marked the first widespread introduction of digital imaging in the hospital. With the advent of powerful computers and the success of CT, other digital imaging modalities have emerged such as ultrasound, nuclear medicine, digital subtraction angiography (DSA) and magnetic resonance imaging (MRI).

In parallel, researchers started evaluating the potential for widespread use of computers in the hospital considering their benefits in acquiring, storing, viewing and communicating diagnostic images. This led to the concept of departmental picture archiving and communication system (PACS) [HEDGE, 86], [NOSIL, 88]. For such systems to be complete in their imaging functions, they have to include the traditional radiographic modality in addition to the existing digital imaging techniques. This objective has stimulated the interest for the digital conversion of traditional radiography. In particular, research work has been focussed on digital radiograph acquisition techniques, on comparative studies of diagnosis performances between analog and digital radiography, and on the use of image processing techniques for image enhancement. Most of this work is related to the imaging of the chest.

2.3 Chest imaging and reviewing

2.3.1 Chest imaging modalities

Chest radiographs are the most frequently performed examinations in hospitals: e.g. at the Civic Hospital of Ottawa, they represent 48% of the total. For diseases of the chest, the radiograph examination is by far the most important examination. Its ability to reveal otherwise unsuspected and undetectable pathologic and physiologic alteration is

unquestioned. The postero-anterior (PA) view which is the standard frontal view, is the basis for routine radiographic evaluation of the chest. Several PA views obtained at different times are commonly used to evaluate the evolution of clinical problems. These retrospect PA examinations sometimes reveal the presence of pathologies which were missed at that time but which are obvious on the most recent PA. Supplementary views are sometimes required to answer specific clinical questions. The lateral view is of value in confirming or clarifying lesions perceived in the frontal projection. Tomograms, in which only one plane of the chest is in focus, are occasionally helpful in separating abnormalities from overlying obscuring structures. CT images have the same purpose and tend also to replace the traditional tomograms.

2.3.2 Chest anatomy overview

In this section, some medical terminology is introduced which relates to the chest anatomy as seen in a postero-anterior (PA) view of a chest . Our intention is to introduce the terms which will be used in the subsequent development of this work.

The PA view is the standard frontal chest radiograph. PA indicates the direction the x-rays travel going through the patient. Fig. 2.1 represents a PA chest view with its main components: the lung field and the mediastinum.

From an anatomical viewpoint, the mediastinum is considered as a region lying between the right and the left lung. However it behaves more like a set of structures which have almost the same radiodensity and merge into a homogeneous shadow superimposed upon that of the spine in the PA projection. The trachea and the heart are part of the mediastinal structures. In the PA projection, the lung field appears as a dark area striped by the ribs and lightened by a bunch of vessels. The hilum is the irregular medial shadow in each lung where the bronchi and pulmonary arteries enter. The thoracic cavity, consisting of the lung field, the mediastinum and the spine is bounded in its lower part by

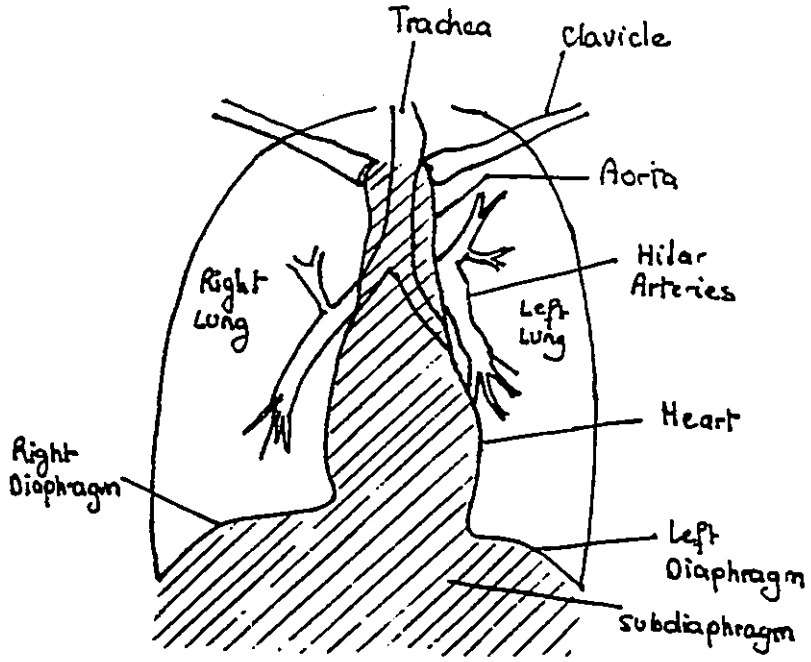

Figure 2.1: PA view of the chest

the diaphragm which marks the separation with the sub-diaphragm area.

Pathologies occurring in a chest may manifest themselves distinctly in the radiograph. An example is *consolidation* where the lung area is filled with some abnormal material. *Air bronchograms* make the trachea and the bronchi appear as air-filled tubular structures and are sometimes accompanied by consolidation. *Interstitial lung disease* involves the actual lung tissue as opposed to the air spaces and is a diffuse lung disease.

Other pathologies may result in signs which are more difficult to perceive. *Nodules*, which are well-defined, dense, more or less round structures, may be small enough to be missed or to raise doubts about their malignity. A *pneumothorax* which refers to free air in the pleural space (the space surrounding the lungs and inside the body wall), sometimes appears as a subtle line on the lung field. Its contrast with the background is not easy to perceive. A *lucency* corresponds to an increase in blackness of an area in the radiograph.

When occurring in the lungs, its visibility may not be clear [FORREST, 82].

2.3.3 What is a good chest radiograph?

The review of a chest radiograph may be impaired by the technical quality of the film. An image will be of satisfactory quality if one can see through the mediastinum and visualize pulmonary vascularity through the lungs [RAVIN, 83]. With an adequately exposed film, one should just be able to visualize the vertebral bodies and intervertebral disk spaces through the heart. The ability to do so suggests that the radiographic exposure is sufficient to allow one to see lesions in the mediastinum as well as in the retrocardiac and retrodiaphragmatic areas. If the vertebral bodies and intervertebral disk spaces are well seen, it is likely that the film is overexposed and that the lung will appear black.

2.3.4 Chest radiograph reviewing

For the review, the radiographs are set up on viewboxes. The viewer, namely the radiologist or physician, first ensures that the film is technically adequate. The exact sequence in which radiographs are reviewed may vary with the individual radiologist or physician. A common habit though, is to start with areas which are of least importance such as the peripheral areas (neck, shoulder, diaphragm), the bones and the soft tissues, and to end with central critical structures such as the mediastinum, the heart and the lungs. Hence, when reading the radiograph, the viewer follows a pathway. If this pathway is the same for every radiograph, it makes easier the detection of perturbations which differ from the usual.

Nodine and Kundel [NODINE, 87] have proposed a general model of visual search and detection based upon measurements of the eye movements of radiologists as they review the radiograph. This model is presented in Fig. 2.2 and assumes that a search task has been defined prior to viewing. The first look at the image provides a global impression

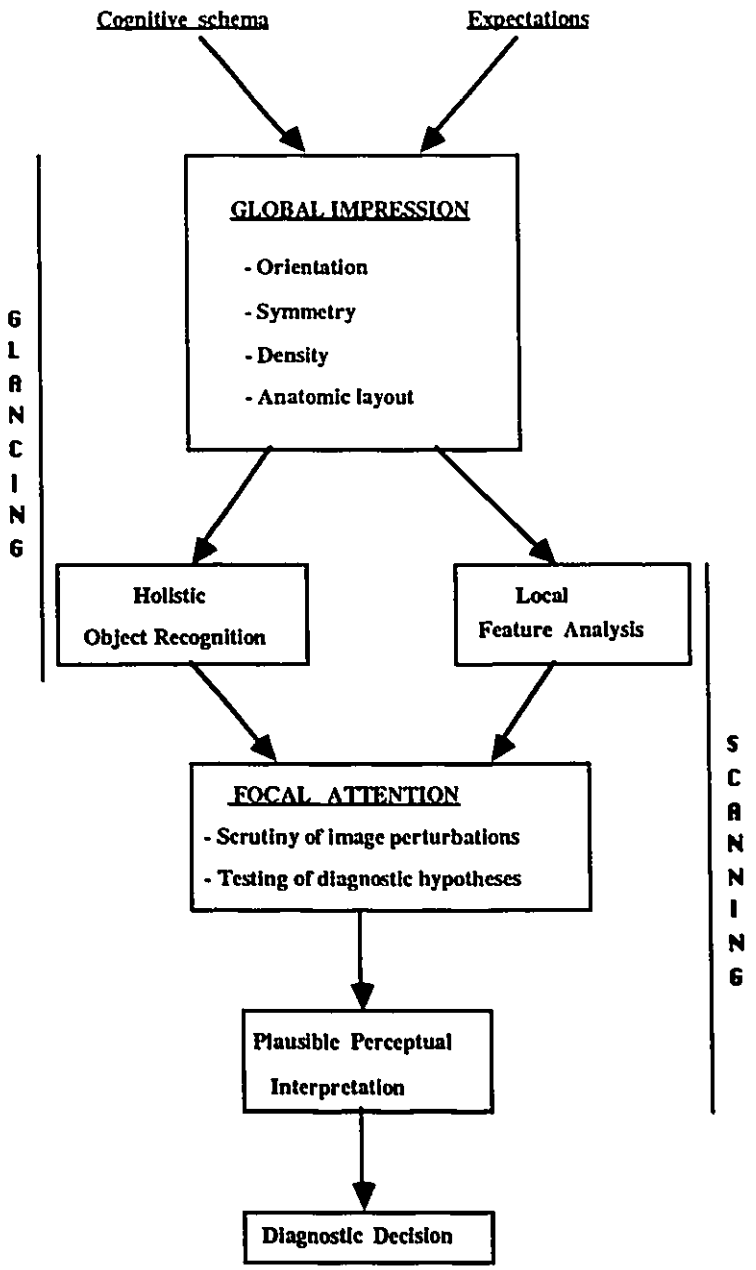

Figure 2.2: Radiograph reviewing (from [NODINE, 87])

which is supported by the medical knowledge of the viewer and which is oriented by its expectations on what has to be seen. In this overall pattern recognition phase, the viewer checks the orientation, the symmetry, the anatomic layout, the global features. The possible perturbations in the image are mentally "flagged". In the scanning stage, the viewer focusses attention on the areas of perturbation which may lead him to another scanning pattern if he feels he has missed some critical information. The final decision is made upon all the local decisions obtained in the scanning phase combined with those of the glancing phase.

2.4 Conventional chest radiography

2.4.1 Film acquisition and characteristics

Conventional chest radiographs are normally made by exposing radiographic film between intensification screens in a cassette or film changer. A latent image results when the silver halides grains of the film emulsion are exposed to the phosphorescence emitted by the image intensification screens and to a minor extent by direct interaction of transmitted x-ray photons with the emulsion (Fig. 2.3). The latent image captured in the film is then developed by chemical processing on the film [MERRIT, 85], [HUANG, 87].

The exposure of the x-ray film is proportional to the product of the milliamperes of x-ray tube current and the exposure time (mAs), it produces film blackening or density. The mAs controls the total number of x-ray in the beam and may be considered analogous to light in producing an ordinary photograph. The measurement of film blackening is called photographic density or density and is defined by:

$$D = \log(I_0/I_t)$$

where D = density, I_0 = light incident on film, I_t = light transmitted by film. Useful densities in radiography range from about 0.3 to 2. The x-ray film presents a pattern of

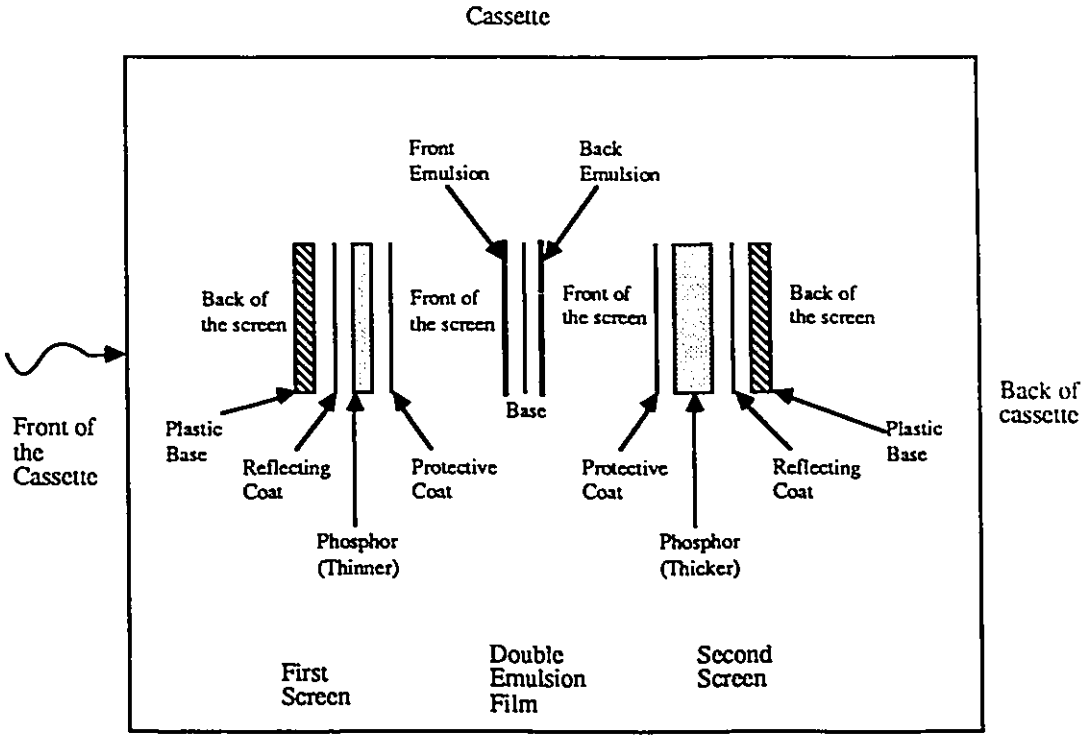

Physical Set Up of a Screen/Film Combination

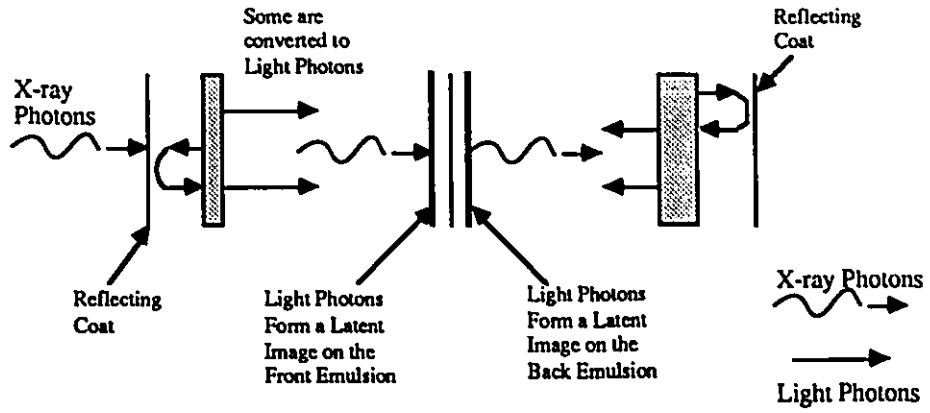

Principle of Operation

Figure 2.3: Film acquisition with image intensification screens (from [HUANG, 87])

variations in optical density, known as radiographic contrast. Radiographic contrast is the density difference between areas in the radiograph and depends on subject contrast and film contrast. Subject contrast is affected by the thickness, density and atomic differences of the subject, the radiation energy (kVp), contrast material and scatter radiation. Film contrast depends on characteristics of the film and the development process.

The ability of the film acquisition system to separate on the x-ray film two closely placed objects is known as spatial resolution. It is usually measured in lines pair per mm. This unity refers to the test pattern (alternate rectangular bar with background of the same width) which is used to quantify the spatial resolution when imaged by the system. The film-screen combination system offers images with excellent spatial resolution: 5 lp/mm.

2.4.2 Analog enhancement

In addition to the modification of some characteristics in the image receptor, the radiograph quality is controlled by the choice of appropriate x-ray energy and the use of anti-scattered grids. Simple post-acquisition enhancements can also be obtained with a bright light and a magnifying glass.

Kilovoltage: The kVp must be selected with care so that the number of photons attenuated by bone and soft tissue are in the proper proportion to produce an x-ray image of high information content. The choice of kVp determines the subject contrast. When low kVp are used, typically 80-90kVp, the radiographs have a high inherent contrast level but are limited in the information they actually present. The radiographs are very "black and white" and tend to accentuate the ribs and outlines of the mediastinal structures. However the pulmonary vascularity and inner structures of the mediastinum are generally obscured. The use of higher values of kVp, namely 120 kVp to 140 kVp, tends to compress the dynamic range of information by reducing the ratio of x-ray photons reaching the film

behind the lungs and the mediastinum. Hence a more satisfactory chest film is obtained. These high kilovoltage techniques are sometimes combined with the use of tailored portal filters which are inserted between the x-ray tube and the patient. Their purpose is to decrease the primary radiation to the lung, thereby increasing the relative mediastinal exposure.

Anti-scatter grids: X-ray photons passing through the patient can create secondary scattered radiations that may also reach the film and affect the image. Scattered radiations are non-informative and degrade the final image by reducing its contrast. The most commonly used anti-scatter device is the x-ray grid.

Enhancement tools: Once the film has been exposed under desired conditions, part of the image content can be enhanced afterwards if the film has been exposed at high kVp. In this case, the film has captured a large amount of information but the eye does not perceive all this information when the film is displayed on a viewbox. Radiologists use a bright spot light to increase the perception at high optical densities (overpenetrated areas) which have been captured. The information at low optical density (underpenetrated areas) is not available. In addition, radiologists sometimes use a magnifying glass to enhance the visibility of small features.

2.5 Digital chest radiography

2.5.1 The digital image

A digital image is a finite two-dimensional matrix of picture elements (pixels) where each pixel has a finite number of density steps or grey levels. There are two approaches to obtaining a digital radiograph: (1) by digitizing a film, (2) by using a direct digital acquisition system.

2.5.2 Image acquisition techniques

Digitization of films

Any conventional radiograph can be digitized by scanning with a video camera, a drum scanner, a solid-state camera or a laser scanner [HUANG, 87]. There are two major advantages to techniques that digitize the information contained in a radiographic film: (1) conventional radiographic techniques, equipment and procedures are employed, (2) the dynamic range of the information contained in the exposed film may be displayed. As seen beforehand, there is in the chest image an extremely wide range of densities because of the wide differences of x-ray attenuation by the lung and by the mediastinum. Even when recorded on the film , this range of information cannot be viewed on a conventional viewbox. If a wide latitude film, i.e. a film capable of acquiring a wide dynamic range, is used, the second advantage is emphasized. These scanning systems provide digital images where the matrix size varies from 512x512 to 4098x4098 with a number of bits per pixel ranging from 8 to 12 [HUANG, 87]. In our experiment we used a laser scanner which provides a 2.82 lp/mm resolution with 10 bits/pixel quantization.

Digital systems

There are three basic approaches to direct digital image acquisition based on x-ray beam geometry: broad-area-beam and scanning beam [GOODMAN, 88].

Broad-area x-ray beam geometry: In the broad area beam approach, the entire object is irradiated at the same time. One of the two techniques used for the sensor is based on the use of photostimulable phosphors coating the large area detector. These special phosphors, when exposed to x-ray, store a portion of the incident energy, which is then released as light by scanning the plate with a focused laser beam. The light is measured and stored digitally in an image array. The spatial resolution of the resulting image

ranges from 2.5 lp/mm to 4 lp/mm with 10 bits/pixel. The second technique, called digital fluorography, makes use of the conventional system of x-ray and image intensifier which is linked to a TV camera. The video output is then transformed into a digital image. The main drawback of this system is its relatively poor spatial resolution (more than 2 lp/mm). The major advantage of the broad-area detectors is their speed of acquisition. In counterpart, they generate a large amount of scatter radiation, though this can be minimized with the use of a grid.

Scanned x-ray beam or scanned projection radiography: The scanned beam approach is based on the transmission of a highly collimated beam of x-ray through the patient onto a radiation sensitive detector. With fan x-ray beam geometry, a scanning linear array of detectors (usually 1024) is used to cover the image area. The projection image is acquired either by moving the patient through a CT-like system or by pivoting the x-ray tube and detector assembly while the patient stands motionless [TESIC, 83]. In a pencil-beam system, a narrow "flying-spot" x-ray beam scans the patient in a raster pattern. The main advantage of these systems is the significant reduction in scatter radiation compared to film-screen systems. The counterpart is an increase in radiation dose to the patient. Besides limited spatial resolution (approximately 1lp/mm), another drawback is the long scanning time required to generate an image. Tesic et al. [TESIC, 83] have extended this technique to a dual energy detector one. This detector can acquire simultaneously an high and a low energy image that can be used to form bone or soft tissues images. These two images can subsequently be processed in a specific way for nodules analysis.

2.5.3 Display conditions

With certain acquisition systems, the digital image can be represented by a matrix as large as 4096x4096 with 12 bits per pixel. The digital images are usually displayed on CRT monitors. Unfortunately, current technology in CRT imposes spatial and contrast

limits to digital imaging. Commonly, CRT systems are capable of displaying 1000x1000 matrices with 8 bits per pixel. Monitors which display 2000x2000 pixels matrices are available but are expensive. When displayed on a 1000 lines CRT monitor, an adult chest image (14" ×17") has a spatial resolution of about 1.5 lp/mm, which is poor in comparison to the 5 lp/mm obtained in conventional radiography. Some observer detection studies have shown that a spatial resolution of 2.5 lp/mm is sufficient for diagnosis [SEELEY, 87]. One possible approach is to scan the image at this resolution, but only to show a portion of it at a time.

2.6 An example of digital radiographic system: the IRIS system

The IRIS system is a multimedia medical communication system developped by the Music Project at the University of Ottawa ([GOLDBERG, 89], [MASTRONARDI, 89]). We describe only the material components related to the imaging aspect. We used this reduced version of the system, which is illustrated in Fig. 2.4, to carry out the experiments and research work which are presented in this thesis.

The images are acquired by digitizing conventional radiograph with a laser scanner manufactured by Konica. For standard chest radiographs, it provides images of size 2000×2430 pixels with 1024 grey levels. The corresponding pixel size is $175\mu m \times 177\mu m$. The scanner also offers the capability of selecting one of four optical density range settings: $(0-4), (0-2), (1-3), (2-4)$. For display requirements, the digitized images are low-pass filtered and sub-sampled to 1000×1200 pixels and the number of grey levels is also reduced from 1024 to 256. The images are displayed on a black and white Philipps monitor at a horizontal scan rate of $84kHz$ with a $104MHz$ band width. This monitor is operated on a portrait style to preserve the aspect ratio of radiographs. An IP-2K Imagraph image memory board of 2 Mbytes is used to refresh the screen at a rate of $60Hz$. All

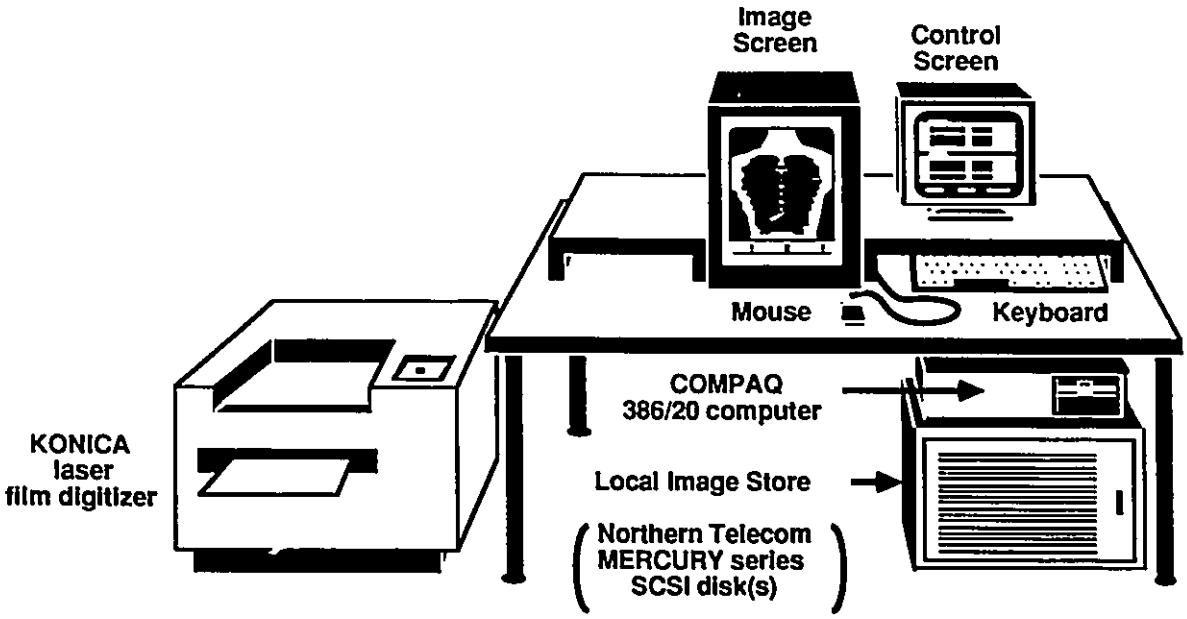

Figure 2.4: Digital imaging components of the IRIS system

these components are controlled by a Compaq Deskpro 386, running at $20MHz$, with 13 Mbytes internal RAM and 130Mbytes of hard disk memory.

2.7 Digital chest radiograph enhancement: task

Digital imaging systems are limited by the spatial resolution they can offer, but this present shortage is compensated by their capability to process the image. Transformations or enhancements on a given image can improve the information visibility and thereby improve the disease detection rate. This is a clear advantage over conventional radiography.

The ideal chest image should render properly all the fine details in the lungs while showing clearly the fine structures in the spine and the vessels behind the mediastinum. However optimal images are not commonplace due to some possible external factors such as the patient anatomy, his health state and the variations in film acquisition techniques. One task of the post-processing is to enhance the overall quality of the image.

Viewing objectives may also decide for the general visibility required in a chest. For instance, if a radiologist wants to check the evolution of a mediastinal disease, he will ask for an image clear in the mediastinum, no matter its likely consequent poor quality in the lung field. Image processing should provide global adaptive enhancement of the image.

Along with the global aspect of an image, the local appearance is also of importance. However the local abnormalities may not be easy to perceive even in images of optimal global quality. This is illustrated by the frequent failure to detect or recognize abnormalities which can be discovered in retrospect. Although the reasons why a lesion is perceptible are complex to determine, some factors have been identified: the lesion configuration (whether it has sharp margins or fuzzy edges), its size, its location and its conspicuity, i.e. the manner in which a single feature within a complex image stands out against the other structures [BROGDON, 83]. Another task of the post-processing must

attempt to enhance locally specific pathologies.

These three enhancement tasks aim at supporting the three-phase procedure involved in viewing a radiograph. We summarize them in Fig. 2.5.

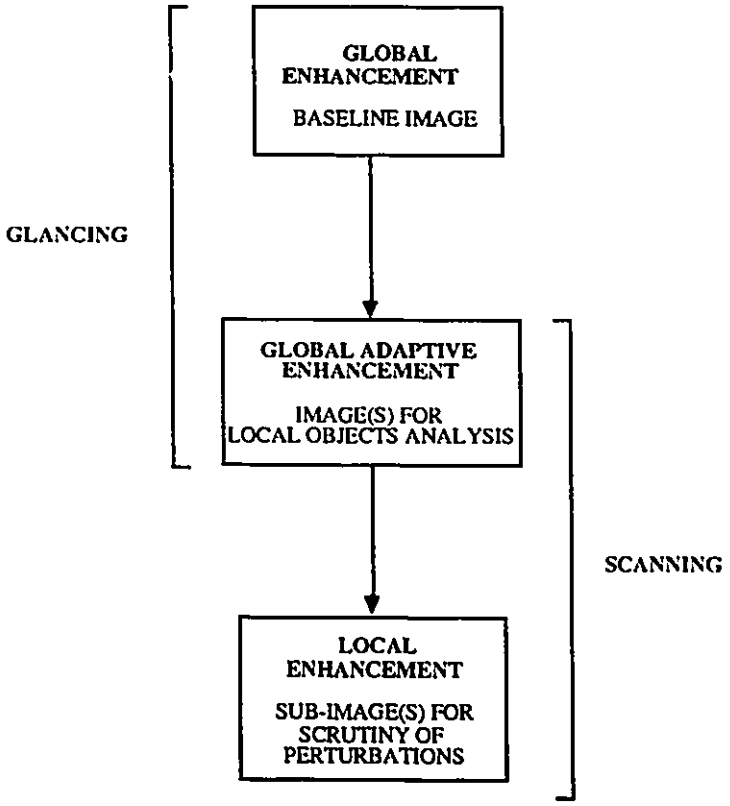

Figure 2.5: Enhancement diagram

2.8 Summary

The attempt to improve radiographic imaging of the chest remains one of the most important and most challenging problems in radiology today. In this chapter, we presented the problems faced in chest radiography and introduced both conventional and digital radiography. We also described the digital radiographic system which we have used for this thesis work. We then defined our task goals for ultimate automatic context-dependent

enhancement.

Chapter 3

A review of enhancement techniques for chest radiographs.

3.1 Introduction

The digital representation of chest radiographs provides the opportunity to enhance the diagnostic potential of the resulting images through the application of processing algorithms. As the human chest is a very difficult structure to image, a great deal of interest has been focussed on specific enhancement techniques for chest images.

In this chapter, we first describe how the enhancement techniques are classified. We then introduce the mathematical terminology which we use in the subsequent review of enhancement techniques for chest images.

3.2 Classifications for enhancement techniques

Image processing operators can be used to perform image enhancement. The enhancement techniques can be categorized on the basis of the properties of their operators. Classifications are based on (1) the operator's sensitivity to the image context, (2) the area which the operator covers, (3) the objective of the operation and (4) the processing method involved.

With respect to the image context, we can recognize the sub-classes *context-free* and

context-sensitive. The operators associated with context-free techniques do not depend on the spatial coordinates and all their parameters are fixed a priori. Conversely, the operators associated with context-sensitive techniques depend on the spatial coordinates and their parameters change according to the local image characteristics.

According to the area covered by the operator, we further sub-divide the techniques into *local* and *global.* Local operators are applied on a subimage whereas global operators are performed on the whole image.

Based on their goals, we can group the enhancement techniques into three non-mutually exclusive classes: (a) noise cleaning, (b) global quality enhancement (c) feature enhancement. In noise-cleaning, the operator aims at removing random noise. For global quality enhancement, the objective is to improve the perceived appearance of the image. In feature enhancement, the goal is to highlight the features of interest.

With respect to the processing methods involved, we decompose the enhancement techniques into 2 groups: (1) spatial sharpening, which involves linear or non-linear spatial domain high-pass filtering for edge-enhancement, (2) grey-level rescaling, which manipulates or requantizes grey levels for contrast enhancement,

In the following review, we will use the classification based on context-sensitivity in which we will differentiate the enhancements according to the type of processing involved.

3.3 Terminology

A digitized image can be defined as a 2D array of integers $g(x,y)$ where $g(x,y)$ is the intensity or the grey level of the pixel at coordinates (x,y). Let I be the entire set of image spatial coordinates. Each pixel $(x,y) \in I$ takes its value in a range defined by the possible grey levels span, $G = [0,m]$ where usually $m = 2^n - 1$.

We note WD a sub-image or subset of the entire set of image spatial coordinates, $WD \subset I$.

We also define

g_{max} as the maximum grey level of the observed image or sub-image,

g_{min} as the minimum grey level of the observed image or sub-image,

g'_{max} as the maximum grey level of the enhanced image or sub-image,

g'_{min} as the minimum grey level of the enhanced image or sub-image,

$H(g)$ as the number of occurrences of pixels with intensity g in the observed image or sub-image,

$h(g)$ as the corresponding normalized histogram: $h(g) = H(g)/nbp$, (nbp is the number of pixels), which approximates the probability distribution function,

$cd(g)$ as the value of the cumulative distribution function of the observed image or sub-image at grey level g, $cd(g) = \sum_{g' \leq g} h(g')$,

$\overline{g}$ as the mean grey value of the whole image or sub-image,

σ as the standard deviation between grey values in the whole image or sub-image,

$W_{n,n}$ as a $n \times n$ matrix of weights and,

$CR(x,y)$ as the contextual region of pixel (x,y), namely the area of given size which surrounds it.

An enhancement technique is a remapping of the intensities of all or part of the pixels described by a mathematical transformation T which yields a new image $g'(x,y)$.

A *context-free enhancement* is defined as

$$g'(x,y) = T[g(x,y)] \quad g(x,y), g'(x,y) \in G \quad (x,y) \in I \tag{3.1}$$

where T, being position invariant, has fixed parameters.

A *context-sensitive enhancement* is expressed as

$$g'(x,y) = T_{CR(x,y)}[g(x,y)] \quad g(x,y), g'(x,y) \in G \quad (x,y) \in I \tag{3.2}$$

where $T_{CR(x,y)}$ is a spatially variant operator which depends on characteristics of the pixel (x,y) and of its contextual region.

A *local enhancement* corresponds to

$$\begin{aligned} g'(x,y) &= T_{WD}[g(x,y)] \quad && (x,y) \in WD \subset I \\ g'(x,y) &= g(x,y) && (x,y) \in I - WD \end{aligned}$$

where T_{WD} depends on characteristics of the window WD.

In the general class of enhancement operators, including either context-free or context-sensitive operators, we further distinguish two types: the spatial operations, denoted T^s, and the contrast transformations, denoted T^c. A spatial transformation alters the grey level value of each pixel depending on the spatial coordinates:

$$g'(x,y) = T^s[g(x,y)] \qquad g(x,y), g'(x,y) \in G \quad (x,y) \in I$$

A contrast transformation operates directly on the grey level values:

$$g' = T^c[g] \qquad g, g' \in G$$

3.4 Context-free techniques

3.4.1 Grey level rescaling: direct transforms

These are used to modify the grey scale of the image by requantizing the grey level values and result in a global contrast enhancement [HALL, 79], [PRATT, 78], [WANG, 83].

Range specification:

This technique is also called *Windowing* in the medical community, as an input and output windows of interest must be specified, respectively (g_{min}, g_{max}) and (g'_{min}, g'_{max}) in the following equation:

$$g' = T^c(g) = \frac{g'_{max} - g'_{min}}{g_{max} - g_{min}}(g - g_{min}) + g'_{min} \tag{3.3}$$

An example is shown in Fig. 3.1.

Statistical differencing:

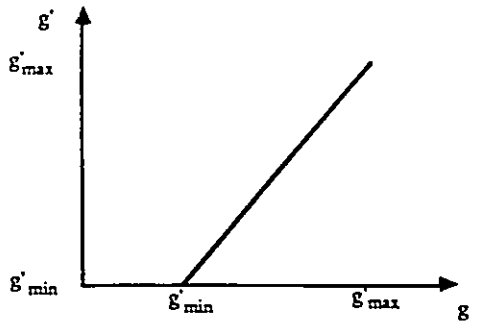

Figure 3.1: Range specification

The eye is more sensitive to changes in image contrast for the middle range of grey levels. As a consequence, it may be useful to change the overall brightness of an image by constraining the mean to a chosen value by the following operation:

$$g' = T^c(g) = g + \overline{g}_{new} - \overline{g}_{old} \tag{3.4}$$

where $\overline{g}_{new}$ is the new mean value and $\overline{g}_{old}$ the old mean value.

The standard deviation can be used to characterize the image contrast. It is a better measure than the minimum and maximum values since it is relatively insensitive to local minima or maxima. An image can be transformed to have a new mean $\overline{g}_{new}$ and a new standard deviation σ_{new}:

$$g' = T^c(g) = \frac{\sigma_{new}}{\sigma_{old}}(g - \overline{g}_{old}) + \overline{g}_{new} \tag{3.5}$$

Statistical differencing can be implemented either as a global or a local operator where the mean and the standard deviation are computed respectively globally or locally. In the case of a local operator, where $\overline{g}_{new}$ and σ_{new} are constrained to be the same throughout the image, the ratio $\sigma_{new}/\sigma_{old}$ may take very large values. Sklansky [SKLANSKY, 78] suggests to replace σ_{old} by $max(\sigma_{old}, t)$ and Pratt [PRATT, 78] by $(\sigma_{old} + t\sigma_{new})$ for some positive t to control the range of allowable values.

Polynomial transformations:

A *3d degree polynomial transformation* has been proposed by O'Gorman et al. [OGORMAN, 85] to stretch the input intensities around a chosen intensity. The extent of the stretching around grey level g_0 is determined by the value of the slope, s, of the remapping function at this point. The coefficients A, B, C, D in the enhancement operator:

$$g' = T^c(g) = Ag^3 + Bg^2 + Cg + D \tag{3.6}$$

are obtained with the following initial conditions:

$$T^c(g_{min}) = g'_{min},\ T^c(g_{max}) = g'_{max},\ \frac{dT^c}{dg}(g_0) = s,\ \frac{d^2T^c}{dg^2}(g_0) = 0$$

If $s < 1$, the low and high ranges of intensities are expanded and the middle range is compressed. If $s > 1$, the middle range of intensities is stretched at the expense of the low and high ranges. Fig. 3.2 shows the possible remappings according to the value of s.

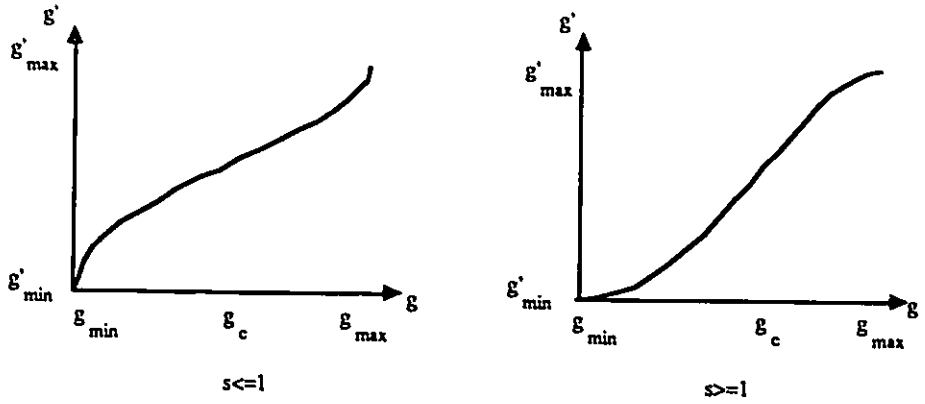

Figure 3.2: Polymomial remapping

Other techniques:

The *logarithmic transformation* is a convenient means for reducing the dynamic range of an image and can be considered as the equivalent of using a bright light on a film

radiograph. The opposite effect is obtained using an *exponential transformation*. For example, a Gamma transformation can be used to cancel the effects of image acquisition non-linearities [HALL, 79].

Other techniques are used for adapting the image to observer viewing preferences. *Grey scale reversal* is a simple example of such a transformation where the image is displayed in the positive mode and is said to facilitate the perception of features in certain areas, such as the lungs and the heart.

3.4.2 Grey level rescaling: histogram based techniques

A second method is based upon transform of the normalized histogram, which is an approximative measure of the *pdf* (*probability distribution function*).

Histogram equalization:

Histogram equalization is the most commonly used histogram transformation. The original grey levels in the image $g, g \in [0, m]$, are mapped into a new set of grey levels $g', g' \in [0, m]$, so that the histogram of the transformed image is as uniform as possible (Fig. 3.3). The enhancement operator is decribed by:

$$g' = T^c(g) = (g'_{max} - g'_{min})CD(g) + g'_{min} \tag{3.7}$$

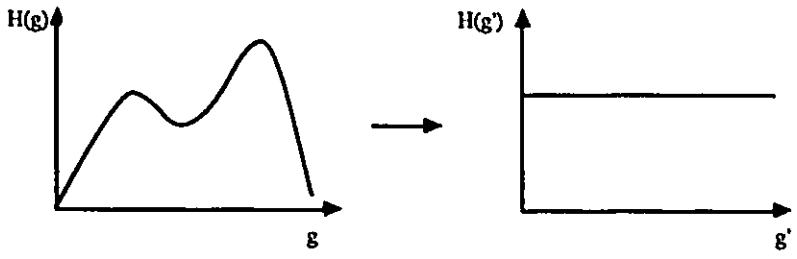

Figure 3.3: Histogram equalization

When $g'_{min} = 0$ and $g'_{max} = m$, histogram equalization is an optimal technique from the information theory viewpoint since it yields the maximal zero-order entropy value.

Hummel [HUMMEL, 77] has proposed an alternative scheme to compensate for the fact that the discrete implementation of histogram equalization does not yield a real uniform histogram. It consists in breaking up the bins which are too high and redistributing them amongst bins which are too low. Suppose that $H(g) = n$ and in this bin n' points must be assigned to grey level g, the remaining $n - n'$ points are chosen randomly from the n points at grey level g and are assigned to $g' + 1$. However, such a redistribution of pixels induces "false" differences and contouring effects.

Histogram hyperbolization:

Histogram hyperbolization has been proposed to take into account the human perception properties. It is intended to produce an image with a uniform distribution of perceived brightness levels. According to a model of brightness perception based on the Weber law [1], Frei [FREI, 77] assumes that the distribution of the displayed brightness levels should be hyperbolic (Fig. 3.4) and expressed by:

$$h(g) = \frac{1}{(g+c)\log(\frac{g'_{max}+c}{g'_{min}+c})} \tag{3.8}$$

The enhancement operator is given by:

$$g' = T^c(g) = (g'_{min} + c)(\frac{g'_{max} + c}{g'_{min} + c})^{cd(g)} - c \tag{3.9}$$

where c can be chosen as a function of the output distribution's slope at point g'_{min} . This technique can be applied either globally or locally.

Histogram specification to a Rayleigh distribution:

Cocklin et al. [COCKLIN, 83] proposed the use of a *histogram specification to a*

[1] $g' = \log(g + c)$ where c is a constant and if g is the original grey level, then g' is the perceived grey level

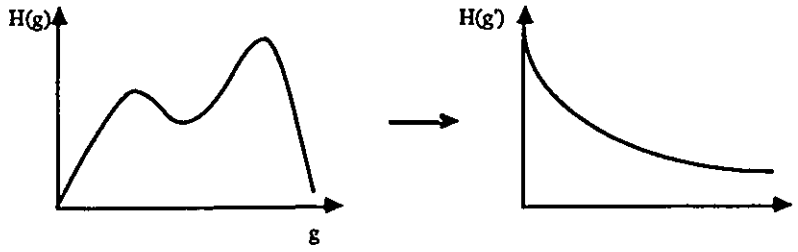

Figure 3.4: Histogram hyperbolization

Rayleigh distribution, $h(g) = g \exp(-g^2/2)$. This transformation supposedly counterbalances the fact that chest distributions are heavily weighted towards the high intensity values (Fig. 3.5). The corresponding transfer function is given by:

$$g' = T^c(g) = g'_{min} + 2a^2 \log(\frac{1}{1 - cd(g)/b}) \tag{3.10}$$

where

$$b = (1 - \exp(-(g'_{max} - g'_{min})^2/2a^2))^{-1}$$

and a is a parameter.

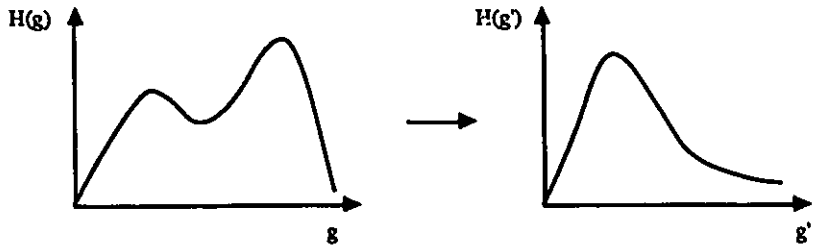

Figure 3.5: Histogram specification to a Rayleigh distribution

3.4.3 Edge enhancement

Edge enhancement attempts to deblur the edge of an object in an image by increasing the grey level difference between the edge pixels of the object and its neighbouring background.

Gradient operators:

Gradient operators are a common form of edge detector which are based on digital approximations of differential equations [HALL, 79]. They are a special case of spatial filtering operators where an high-pass filter $W(x,y)$ is operated on the input image $g(x,y)$ in the following way:

$$g'(x,y) = T^s(g(x,y)) = g(x,y) * W(x,y) \tag{3.11}$$

where $*$ is the convolution operator.

In practice, the point spread function of the filter is truncated and consequently we end up with a finite convolution:

$$g'(x,y) = T^s(g(x,y)) = \sum_{i=0}^{N}\sum_{j=0}^{M} g(x+i-[N/2], y+j-[M/2])W(i,j) \tag{3.12}$$

where $N \times M$ is the size of the mask W.

Daponte and Fox [DAPONTE, 88] have investigated the application of gradient operators to plain film chest X-rays. In particular, they considered the Sobel and Roberts gradient operators expressed by the sum of the results of applying two orientation sensitive convolution windows:

Sobel operator

$$W^1_{3,3} = \begin{bmatrix} -1 & 0 & 1 \\ -2 & \underline{0} & 2 \\ -1 & 0 & 1 \end{bmatrix} \tag{3.13}$$

and

$$W^2_{3,3} = \begin{bmatrix} -1 & -2 & -1 \\ 0 & \underline{0} & 0 \\ 1 & 2 & 1 \end{bmatrix} \tag{3.14}$$

Roberts operator

$$W^1_{2,2} = \begin{bmatrix} 0 & 1 \\ -1 & \underline{0} \end{bmatrix} \tag{3.15}$$

and

$$W^2_{2,2} = \begin{bmatrix} -1 & 0 \\ 0 & \underline{1} \end{bmatrix} \tag{3.16}$$

The underlined elements correspond to the center of the convolution window.

A drawback with gradient operators is that they enhance image noise along with edge objects, so that it may be useful to apply a noise reduction filter prior to the edge detection operator. Good results for chest radiographs are reported with a combination of 3×3 Gaussian filter (for noise reduction) followed by the Sobel operator (for edge enhancement).

Cocklin and Kaye [COCKLIN, 82a] have proposed a dedicated edge enhancement scheme for pneumothoraces. A pneumothorax refers to the presence of gas in the space between the lung and the chest wall. It appears as a slight difference between the density of the gas in the pleural cavity and the density of the air filled lung tissue. Pneumothoraces are often very subtle. Cocklin and Kaye propose to enhance the conspicuity of pneumothoraces either with simple unidirectional edge detectors or with an operator detecting edges in any likely orientations. To detect a vertical pneumothorax, they use the following convolution mask:

$$W^v_{5,5} = \begin{bmatrix} -1 & 0 & 0 & 0 & 1 \\ -1 & 0 & 0 & 0 & 1 \\ -1 & 0 & \underline{0} & 0 & 1 \\ -1 & 0 & 0 & 0 & 1 \\ -1 & 0 & 0 & 0 & 1 \end{bmatrix}$$

To detect the pneumothoraces which present an horizontal or a diagonal edge shadow, the following mask is more adapted:

$$W^d_{5,5} = \begin{bmatrix} 0 & 0 & 1 & 1 & 0 \\ 0 & 0 & 0 & 1 & 1 \\ -1 & 0 & \underline{0} & 0 & 1 \\ -1 & -1 & 0 & 0 & 0 \\ 0 & -1 & -1 & -1 & 0 \end{bmatrix}$$

To enable edges in vertical, horizontal and diagonal direction to be detected, a simple sum of the results of applying each of the convolution mask W^v, W^d and a transpose of W^v may be used.

Unsharp Masking

Another approach to edge enhancement in the case of chest radiographs is the use of *Unsharp Masking*. The photographic technique of unsharp masking consists in superimposing a slightly out of focus negative on the original positive [GONZALES, 77] which can be represented as:

$$g'(x,y) = T^s(g(x,y)) = a(g(x,y) - \overline{g}_{n,n}(x,y)) + \overline{g}_{n,n}(x,y) \tag{3.17}$$

where a is a gain factor, $\overline{g}_{n,n}(x,y)$ is a low-pass filtered version of $g(x,y)$ obtained with a $n \times n$ filter mask. This equation preserves the local mean in the image. If a is too large, a ringing artifact may appear at sharp edges. To reduce this effect, Schwartz and Soha [SCHWARTZ, 77] have proposed the *threshold zonal filtering* technique. In the computation of the local mean, the only neighboring pixels of (x,y) which are used are those which satisfy the relation:

$$|g(i,j) - g(x,y)| \leq T(x,y),$$

where T is a threshold. Cocklin et al. [COCKLIN, 82] propose an alternative method based on a relaxed form of the original equation:

$$g'(x,y) = T^s(g(x,y)) = g(x,y) + c(a-1)(g(x,y) - \overline{g}_{n,n}(x,y)) \tag{3.18}$$

where $0 \leq c \leq 1$ and a is either held fixed or is related to the local deviation $g(x,y) - \overline{g}_{n,n}(x,y)$.

Jackson and Kaye [JACKSON, 82] have pointed out that, besides overenhancing edges which are well defined in the original image, unsharp masking also has the drawback of enhancing noise. Their proposed *weighted unsharp mask* is a generalization of the *threshold zonal filtering* technique. To eliminate the amplification of low-level noise, they retain for the local mean computation the neighbouring pixels of (x,y) which satisfy the relation:

$$V_1 \leq |g(i,j) - g(x,y)| \leq V_2$$

where V_1 and V_2 are positive threshold values. To suppress the enhancement of large intensity variations, they impose a weight factor of 1 on the low-pass mask when

$$D = |g(i,j) - g(x,y)| \leq N$$

and a weight factor of

$$(0.5 + k)/(D + k)$$

when $D > N$, rather than setting this last term to 0 as in the threshold zonal filtering approach.

3.5 Context-sensitive techniques

Context-sensitive operators adapt to the variations in image context. As chest images show areas with widely different characteristics, context-sensitive operator are theoritically very appealing. Two main groups of context-sensitive enhancement emerge in the literature: histogram directed processing (including adaptive filtration) and adaptive histogram equalization.

3.5.1 Histogram directed processing

A chest image globally contains two different areas, the lung field and the mediastinum which have to be processed selectively. McAdams et al. [MCADAMS, 86] have shown that the histogram of the thoracic cavity in a chest radiograph is essentially bimodal, each mode corresponding respectively to the lung field and the mediastinum. From this property, they proved that a reasonable grey level threshold can be determined to select one or the other area. As a consequence, simple grey scale transform can be achieved to selectively enhance these areas. For instance, McAdams et al. proposed a "dual-slope" transform (Fig. 3.6) and a "V" transform (Fig. 3.7).

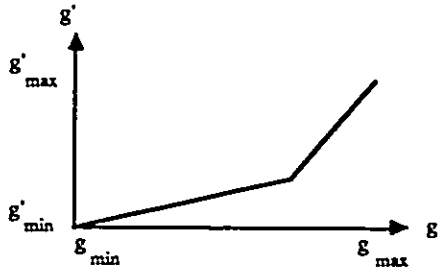

Figure 3.6: Dual-slope transform

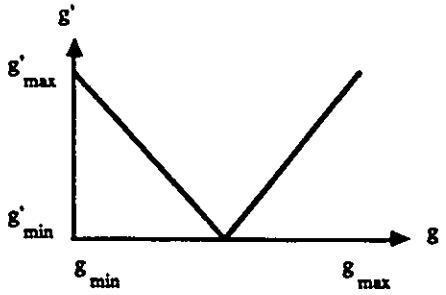

Figure 3.7: "V" transform

The first method enhances vertebral column detail, retrocardiac vessels and bronchial structure of the mediastinum and compresses the contrast in the lung field. The "V" transform achieves simultaneous contrast expansion of the mediastinum and the lung field with grey scale inversion of the lung field.

McAdams et al. [MCADAMS, 87] also investigated modifying unsharp masking so that it is context-sensitive. Their goal is to enhance selectively the mediastinum without enhancing the lung field. In Equ. 3.17, the coefficient a now varies with the area under consideration. The value for a is configured according to the grey level threshold for the lung field-mediastinum separation as shown in Fig. 3.8. For the low-pass filtered image

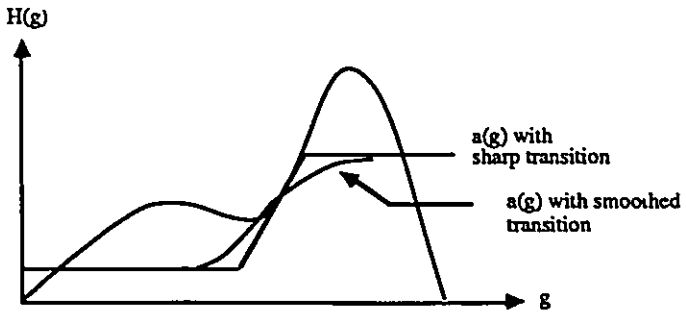

Figure 3.8: Histogram directed processing

computation, they investigated the use of different sizes for the convolution window. They concluded that a size of 100×100 yielded the best results. They also pointed out that, to avoid ringing artifacts, a, rather than being a step function of grey level intensity should be configured with smooth transitions (Fig. 3.8).

3.5.2 Adaptive histogram equalization

The adaptive histogram equalization (*AHE*) technique was proposed in its basic form by Ketchman [KETCHMAN, 76], Hummel [HUMMEL, 77] and Pizer [PIZER, 81]. *AHE* involves applying to each pixel the histogram equalization mapping based on the pixels

in a surrounding region. This neighbcurhood region is commonly called the contextual region (CR) (Fig. 3.9). The transform is expressed as follows:

$$g'(x,y) = T_{CR(x,y)}[g(x,y)] = g'_{min} + (g'_{max} - g'_{min})h_{CR(x,y)}(g(x,y)) \qquad (3.19)$$

where $h_{CR(x,y)}(g(x,y))$ is the frequency of occurrence of grey level value $g(x,y)$ within the contextual region CR.

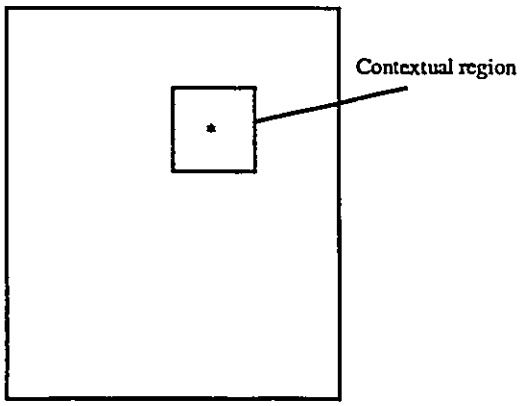

Figure 3.9: Contextual region in AHE

The contextual regions may be disjoint or overlapping. In the former, there are problems related to continuity of the transformations at the boundaries, which are attenuated by using overlapping regions [PIZER, 87].

The main drawback of *AHE*, as described here, is its high cost in computing time. Pizer et al. [PIZER, 87] propose to speed up the process by calculating the desired mapping only at a sample of pixels and interpolating the mapping between these sample locations. These authors state that for a wide range of medical images an optimal CR area is between 1/16 and 1/64 of the image, which is a trade off between improving contrast of features and limiting the influence of noise. Pizer et al. [PIZER, 87] have also proposed a variation on *AHE* called clipped *AHE* (*CLAHE*) which limits noise amplification in relatively homogeneous regions. A variation on contrast enhancement is obtained by

modifying the slope of the mapping function of the input intensity values to the output ones. In histogram equalization, this slope is proportional to the height of the histogram for any input grey level. Furthermore, homogeneous areas correspond to high peaks in the histogram. Therefore, prior to histogram equalizing, a clipping of the histogram values beyond a certain level C limits the contrast enhancement for these intensities (Fig. 3.10).

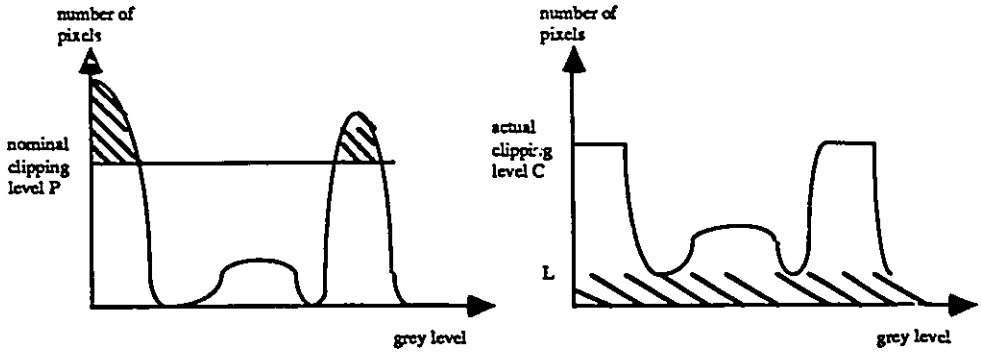

Figure 3.10: Histogram clipping in *CLAHE*

The clipped values are redistributed uniformly through the histogram. The authors indicate that the clipping level C must vary with the imaging modalities and body region imaged.

Vossopoel et al. [VOSSEPOEL, 88] propose a different approach to preventing excessive noise amplification in CR's showing pronounced peaks. The histogram of a CR with a high peak is refined by a linear combination of the histogram of one or more neighbouring CR's.

The previously cited authors have essentially studied the applications of adaptive *HE* to computed tomography (CT) images. Sherrier and Johnson [SHERRIER, 87] report the application of adaptive histogram equalization *AHE* for plain chest radiographs, to which two constraints are imposed:

1. The mediastinum and the subdiaphragm must be enhanced selectively with little

processing in the lung field.

2. The transition between processed and unprocessed areas must be smooth and free of artifacts.

The image is basically divided into four zones depending upon the median or mean of the CR:

1. the lung field,
2. the mediastinum,
3. the transition area between lung field and mediastinum,
4. the subdiaphragmatic area.

The sample points are remapped differently according to the zone to which they belong. A sample point in the lung field is not altered. A sample point in the mediastinum is remapped as in *AHE*. A sample point in a transition area is remapped as in *AHE* if the mean of its CR is more than a given threshold, otherwise it is not processed. This allows to control ringing artifact at the transition border. In the subdiaphragmatic area where the noise level is high, histogram equalization is performed but to a limited range of the available grey level scale. The pixels in either zone which are not sample points are mapped as in *AHE* by bilinear interpolation.

3.6 Summary

A variety of techniques for the enhancement of chest images have been introduced. Because of the complex nature of chest images, an enhancement technique which is *context-free*, is likely to succeed for a given viewing task but not for all of them. Some authors have proposed *context-sensitive* techniques to display optimally the whole chest image. However, none have reported about the efficiency of these techniques as judged by the ultimate viewers and experts, namely the physicians and the radiologists.

Chapter 4

Subjective Evaluation of Global Enhancements

4.1 Introduction

As we have seen in Section 2.3.4, there are three phases in viewing a radiograph. The first phase corresponds to the "gestalt" or to getting a global impression. The second phase consists in analysing the objects and the local features (e.g. size and borders of the heart, lung vessels). The third phase refers to focal attention and scrutiny of the perturbations (e.g. shape and density of small nodules). To support these three different phases, three different types of enhancement procedures are proposed. The role of the first is to yield an appropriate compromise or baseline image matched to the "gestalt" requirement. The second enhancement is then invoked to aid in the analysis of local features. Finally, various local enhancements are then called to highlight the areas of interest.

In this chapter, we focus on the first two enhancement phases as applied to digitized chest radiographs. We first introduce our objectives and describe the material and methods for user evaluation trials. For the first phase, we report results on user evaluation trials of different enhancements that are applied to the original digitized images to yield baseline images. For the second phase, we report on the performance of simple global adaptive grey-scale manipulations to support local feature analysis, specifically for the lung, the

heart and the spine. In addition we report results of user trials on the applicability of various grey level reversal transformations.

4.2 Objectives

The objectives of the subjective evaluation tests for global enhancements were as follows:

- Determine the appearance of the first overview image.
- Determine the usefulness of global adpative enhancements for local features analysis.
- Determine the effectiveness of reverse mode transformations.

4.3 Material and Methods

The hardware components which were used to prepare these experiments were presented in Section 2.6. The software was written in the "C" programming language and run under the MS-DOS operating system.

The experiments were carried out in collaboration with the Department of Radiological Sciences at the Ottawa Civic Hospital a 950 bed tertiary care teaching hospital affiliated with the University of Ottawa.

Our chest images were selected from three different departments of the hospital where different acquisition techniques are used. In the Emergency Department, images are exposed at 90 Kvp. The same amount of energy is used in the Intensive Cares Unit but the images have disproportionate shapes as patient positions are difficult to control. Images from these two departments were digitized with a reading setting of $(0-2)$. In the Radiology Department, images are exposed at 145 Kvp and an anatomically shaped filter is used to reduce the amount of energy going through the lung. As a result, the lung area, the mediastinum and subdiaphragmatic areas are equally contrasted. These radiographs

were digitized with a reading setting of $(0-4)$. Two PA images were obtained from each department and constitute the test-set.

The whole experiment was decomposed into three sub-experiments according to each one of the previously defined objectives:

- Optimization of the first overview image.
- Enhancements for local features analysis.
- Reverse mode transformations.

4.4 Experiment1: Optimization of the first overview image

4.4.1 Objective

The objective of this first experiment is to find the best baseline image. By baseline image, we mean the first image displayed on the screen and read by the user during the "gestalt" phase. In particular, we want to answer the following questions:

- What is the enhancement that yields the "best" baseline image?
- Do the preferences vary from radiologists to other clinicians?
- Do the preferences depend upon the radiograph acquisition technique?
- How do the preferred baseline images compare with the analog films?

We are only interested in the physician's first impression on the displayed image, assuming that he does not know anything about the analog film or about the patient's history.

4.4.2 Transformations

Although our images are digitized to 1024 contrast levels, corresponding to 10 bits, our workstations only offer a range from 0 to 255. The baseline images are obtained by transforming the digitized images with 1024 grey levels to images with 256 grey levels. In all six types of transformations [COCKLIN, 83], [MCADAMS, 86], [SMATHERS, 85] are tested with A, B, C, D being normalization factors:

1- Simple truncation,

$$T(g) = Int(\frac{255}{1023}g),$$

where Int is the integral part of g

2-Exponential and power functions, which expand the higher end of the scale,

$$T(g) = Int(A\exp(g)) \text{ or } T(g) = Int(Bg^n)$$

3- Logarithmic and n-th root functions, which expand the lower end of the scale,

$$T(g) = Int(C\log(g)) \text{ or } T(g) = Int(Dg^{1/n})$$

4- Piecewise linear functions which expand either the first or the last part of the scale,

$$T(g) = \begin{cases} Int(A.g) & \text{if } x \in [0, M] \\ Int(Bg + C) & \text{if } x \in]M, 1023] \end{cases}$$

5- Polynomial fonctions and piecewise non linear fuction, which expand the middle part of the scale,

$$T(g) = Int(Ag^3 + Bg^2 + Cg + D)$$

or

$$T(g) = \begin{cases} Int(T1(g)) & \text{if } g \in [0, M] \\ Int(T2(g)) & \text{if } g \in]M, 1023] \end{cases}$$

6- Global histogram equalization, which equalizes the grey level distribution and stretches the contrast in low-contrasted areas,

$$T(g) = Int(A.cd(g)),$$

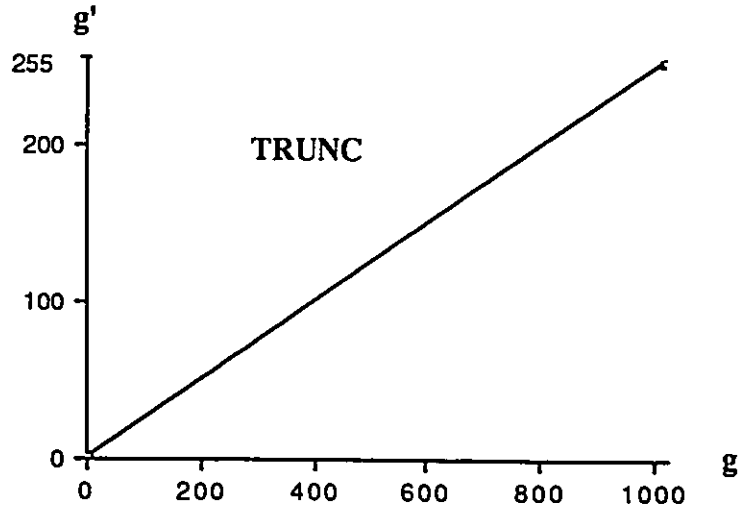

Figure 4.1: Simple truncation

where $cd(g)$ is the cumulative distribution function.

We now provide additional information about the particular form of transformation employed and its intended effect. We note that transformation 1 (Fig. 4.1) has no enhancement effect. For both, transformations 2 and 3, n is set equal to 2. The effect of transformation 2 is to enhance the bright areas and contract the dark areas (Fig. 4.2). Effectively this enhances the heart and spine and de-emphasizes the lung field. These effects are reversed in the case of transformation 3 (Fig. 4.3). For transformation 4, we chose to expand the lower end of the scale and chose as a breakpoint the mean grey level value (Fig. 4.4). This preferentiably enhances the lung field. A transformation of type 5 can be chosen to operate on the middle range of grey levels and leaves the low and high ends contracted. This is implemented by choosing the mean grey level value as a breakpoint and concatening a square function and a square-root function about this breakpoint (Fig. 4.5). Finally, the transformation 6 theoretically equalizes the contrast throughout

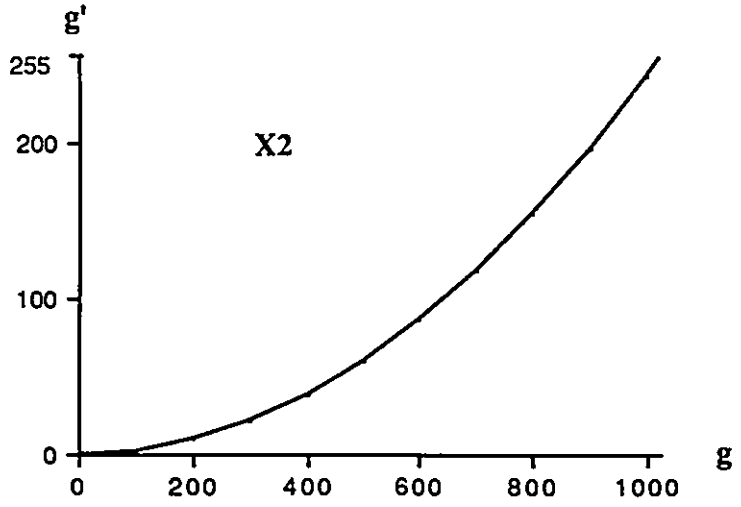

Figure 4.2: Square transformation

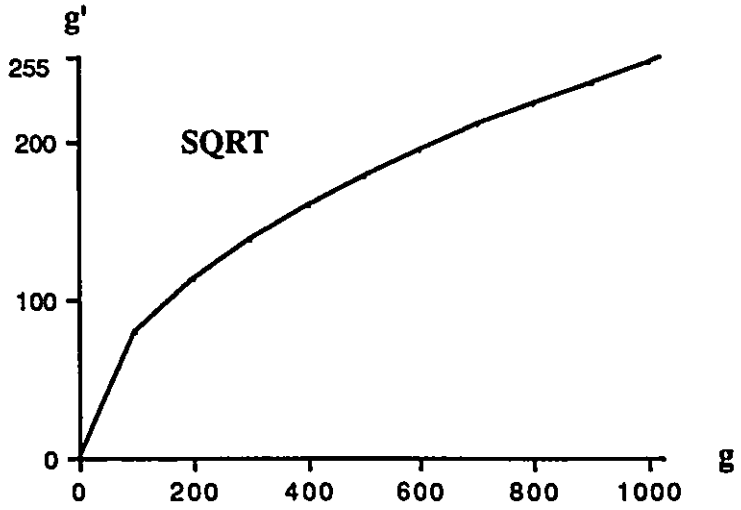

Figure 4.3: Square root transformation

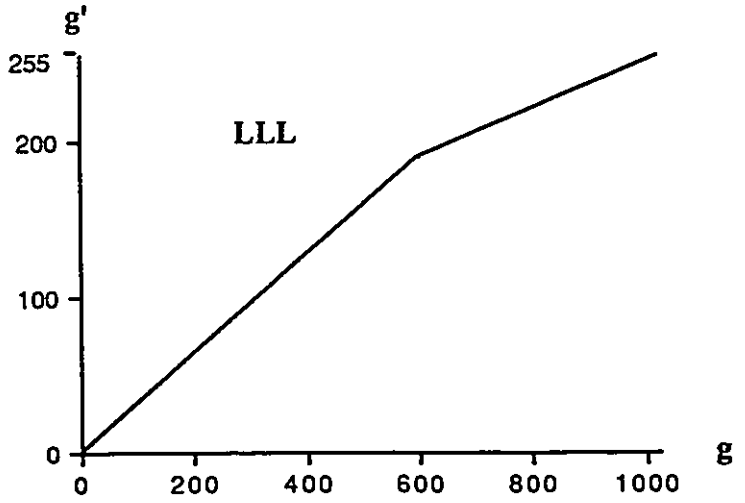

Figure 4.4: Piecewise linear transformation.

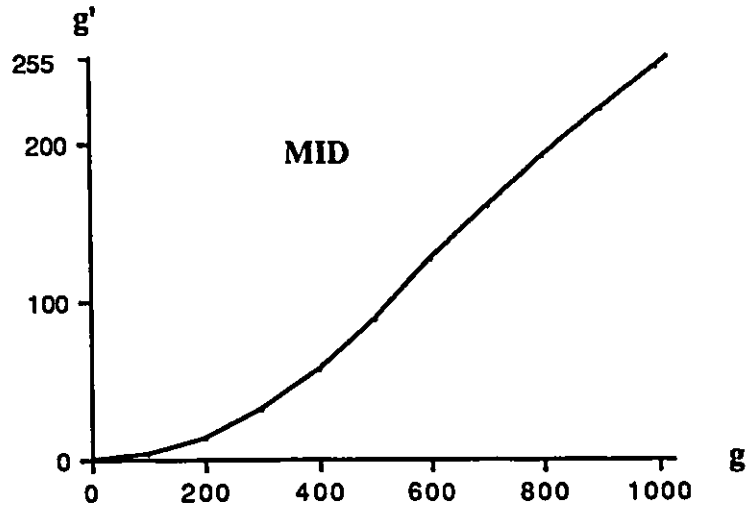

Figure 4.5: Middle-range stretching

the image.

4.4.3 Method

Two series of tests were conducted, the first to determine the "best" baseline image and the second to compare this baseline image to the original analog film. In the first series, six possible baseline images are proposed for each image. These tests were run in a paired-comparison task [COOMBS, 70] leading gradually to the final selection. Twenty-one physicians participated in the test: six emergentologists and fifteen radiologists. This last group included both board-certified radiologists as well as resident radiologists. For the second series of tests, the best baseline images are compared to the corresponding analog films by using a scale varying from -1 to $+1$, where -1 is less clear, 0 is the same, $+1$ is more clear. This latter series involved six radiologists and four emergentologists.

4.4.4 Results

The results of the first tests are listed in Table 1-1 and show for each image and for each physician the transformation rated as best.

What is the enhancement that yields the best baseline image?

Radiology Department images:

For the first image (RAD1), the mean-range stretching (MID) is the preferred transformation in 75% of the cases. For the second image (RAD2), the two preferred transformations are the square function (X2) and the mean-range stretching (MID).

We note that for these two images, the breakpoint which corresponds to the mean value is fairly high (767, 721). The two preferred remappings are therefore very similar. In effect, the corresponding analog films presented good contrast both through the lung field and the mediastinum area. The two remappings provided digital baseline images close to the analog film. In particular, the lung field showed up clearly.

	RAD1	RAD2	EM1	EM2	ICU1	ICU2
RADIOLOGISTS						
1	LLL	TRUNC	TRUNC	TRUNC	TRUNC	LLL
2	MID	X2	MID	TRUNC	EQU	LLL
3	MID	X2	X2	EQU	MID	TRUNC
4	MID	MID	X2	EQU	MID	LLL
5	MID	MID	X2	MID	EQU	LLL
6	MID	X2	EQU	X2	X2	MID
7	MID	MID	MID	EQU	TRUNC	LLL
8	MID	MID	X2	X2	TRUNC	TRUNC
9	X2	X2	X2	X2	MID	SQRT
10	MID	MID	X2	EQU	TRUNC	SQRT
11	MID	MID	X2	TRUNC	TRUNC	SQRT
12	MID	X2	MID	X2	TRUNC	LLL
13	MID	MID	X2	X2	MID	TRUNC
14	X2	X2	MID	TRUNC	TRUNC	LLL
15	MID	X2	MID	X2	MID	LLL
EMERGENTOLOGISTS						
1	X2	MID	MID	TRUNC	TRUNC	LLL
2	MID	MID	X2	EQU	MID	LLL
3	X2	X2	X2	EQU	EQU	TRUNC
4	MID	X2	MID	MID	MID	LLL
5	MID	X2	TRUNC	TRUNC	MID	TRUNC
6	MID	X2	X2	EQU	MID	TRUNC

Table 4.1: Results of Experiment 1 for the baseline image

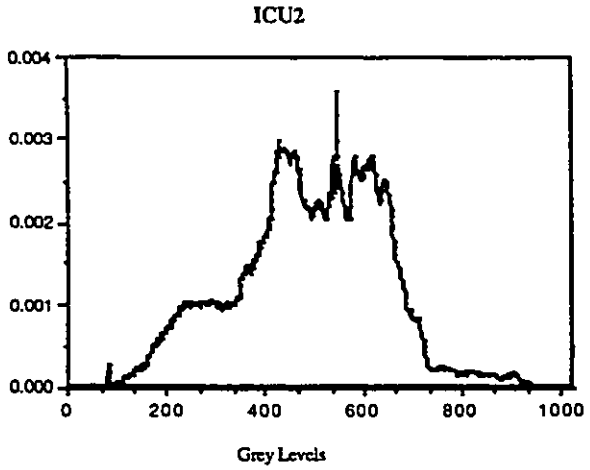

Figure 4.6: Image ICU2 grey level distribution

Emergency Department images:

For the first image (EM1), the two preferred transformations are the square transformation (X2) and the mean-range streching (MID). For the second image (EM2), the histogram equalization (EQU) and the square function (X2) are preferred. This image shows an overspread disease through the lung field which causes it to appear as white and washed-out. The main effect of the histogram equalization is to accentuate the contrast through the lung field.

ICU images:

For the first image (ICU1), preferences go from the mean-range stretching (MID) in 42% of the cases to simple truncation (TRUNC) in 38% of the cases. For the second image, half of the physicians selected the piecewise linear transformation (LLL) which stretch the contrast through the lung field. We note that in this case the original image has a centered and fairly symmetric grey level distribution (Fig. 4.6).

These results, analysed image by image and supported by the physicians' comments, show that the selection of preferred images is led by a common priority: getting satisfac-

tiory visibility in the lung field.

Hence the baseline image judged as giving the best global impression is an image which preferrably enhances the lung field.

Do the preferences vary from radiologists to emergentologists?

Table 4.1 shows clearly that **radiologists'choices and emergentologists'choices are highly correlated.** Both the radiologists and the emergentologists chose images where the best advantage was given to the lungs.

Do the preferences depend upon the radiograph acquisition technique?

Yes definitely, but they also appear to correlate with image quality. In effect, Table 1-1 shows that the preferred transformations depend upon the film acquisition. However, when images are of good quality such as RAD1, RAD2, EM1, there seems to be a clear trend for the transformations X2 and MID. For the other images, the trend is more difficult to deduce.

	RAD1		RAD2		EM1		EM2		ICU1		ICU2	
	M	SD	M	SD	M	SD	M	SD	M	SD	M	SD
BASELINE VS FILM	-0.62	0.48	-1	0	-0.16	0.83	-1	0	-1	0	-0.33	0.66

Table 4.2: Comparison between the baseline image and the film

How do the preferred baseline images compare with the analog films?

Table 4.2 shows how the digitized enhanced image is evaluated in comparison to the analog film. The scale varies from -1 to $+1$ where -1 is less clear, 0 is the same and $+1$ more clear.

In general, the analog film is preferred, however, in some cases the baseline image is rated by the physicians to be as good as or better than the analog film.

4.5 Experiment 2: Enhancements for local features analysis

4.5.1 Objective

The objective of this experiment is to judge the effectiveness of simple global adaptive enhancements for the second phase in viewing a radiograph, i.e. local features analysis. Attention is focussed on the lungs, the heart and the spine. We note that as features of interest are quite large, global adaptive enhancements are employed. The questions that we want to answer are as follows:

- How are the visibilities of the lung field, the heart and the spine rated in the baseline images and in the global adaptive enhanced images?
- How do the enhanced digitized images compare with the analog film in terms of image analysis effectiveness?

4.5.2 Transformations

In literature, piecewise linear transformations have been proposed to stretch the low and high ranges [MCADAMS, 86]. We select one such transformation to improve the visibility in the lungs and another for the mediastinum (spine and heart areas):

Low-range stretching is used for the lungs:

$$T(g) = \begin{cases} Int(\frac{190}{M}g) & \text{if } g \in [0, M] \\ Int(\frac{65}{255-M}(g-M)+190) & \text{if } g \in]M, 255] \end{cases}$$

High-range stretching is used for the mediastinum:

$$T(g) = \begin{cases} Int(\frac{65}{M}g) & \text{if } g \in [0, M] \\ Int(\frac{190}{255-M}(g-M)+65) & \text{if } g \in]M, 255] \end{cases}$$

In both these transformations, g is a grey level value, Int is the integral part and M is a breakpoint which is set to the mean of the grey level values corresponding to the

thoracic cavity of the chest. These 8 bits to 8 bits remappings are performed by simply changing the look-up table values of the display.

4.5.3 Method

The six best baseline images chosen in Experiment 1 are used as the test-set. The physicians rate the clarity of information for the baseline image and for the images processed by the high-stretch and the low-stretch transformations.

A ranking on a scale from 1 to 5 is used, where 1 is not at all clear and 5 is very clear. A comparison session follows in which the best baseline image and the two processed images are compared with the analog film. A ranking on a scale from -3 to $+3$ is used, where -3 is much less clear, 0 is the same and $+3$ is much more clear. The tests involved ten physicians: six radiologists and four emergentologists.

4.5.4 Results

How are the visibilities of the lungs, the heart and the spine rated in the baseline image and in the global adaptive enhanced images?

The results are listed in table 4.3 in terms of mean and standard deviation of rankings (between 1 and 5) for each image, each transformation and the three features of interest: lungs, heart and spine.

For the lungs, the baseline images yields the best visibility. The heart is also more visible in the baseline images. For the spine, the high-range stretching yields the preferred images.

All the physicians agreed on the good visibility of the lung field in the baseline images. On some images however, better visibility is asked for the bases and periphery of the lungs. Image EM2 showed a general pathology in the lung field which explains its mediocre score. The low-range stretching does not improve the general visibility of the lung field. Although

the lung markings are enhanced, the physicians feel that they miss some information at the periphery of the lungs. The baseline image is rated as a good image for the heart. A general trend in the comments is to ask for more visibility through the heart and on its borders to bring out the margins. The heart is not improved by the low-range stretching. The high-range stretching accentuates the contrast through it but tends to make its borders vanished. The visibility of the spine is poor in the baseline image. The radiologists indicated the need to see more clearly the *pedicles*, the *spinus process* and the *disk spaces*. The high-range stretching enhances the spine and these inner features are clearly brought out.

Hence the baseline images are appropriate for the lung field and for the heart. The low-range stretching and the high-range stretching respectively enhance the inner part of the lungs and of the heart. The high-range stretching clearly brings out the spine.

		RAD1		RAD2		EM1		EM2		ICU1		ICU2	
		M	SD	M	SD	M	SD	M	SD	M	SD	M	SD
BASELINE	Lungs	4.42	0.56	5	0	4	0.81	3	0.81	4.2	0.4	4	0.57
	Heart	4.87	0	4.5	0.7	4.16	0.72	3	0	3.8	0.4	4	0.57
	Spine	2	0.53	3	0	2.5	0.76	3.33	0.05	3.8	0.74	3.33	0.75
LOW-STRETCH	Lungs	4	0.75	4.5	0.7	3	1	1.66	0.05	4	0	3.83	0.4
	Heart	4.14	1	4	0	3.5	0.76	1.66	0.05	3.4	0.8	3.33	0.75
	Spine	1.71	0.88	2	0	1.83	0.69	1.66	0.05	2.6	0.8	2.33	0.47
HIGH-STRETCH	Lungs	2.29	0.68	3	1	2.33	0.48	2.33	0.47	1.2	0.4	2.5	0.95
	Heart	3.57	0.73	4	1	4	1.15	3.66	0.5	4	0.63	3.66	0.51
	Spine	3.57	0.5	4.5	0.7	3.66	0.77	4	0	4.4	0.49	4.33	0.5

Table 4.3: Results of experiment 2 for the enhanced images

How do the enhanced digitized images compare with the analog film in terms of image

		RAD1		RAD2		EM1		EM2		ICU1		ICU2	
		M	SD	M	SD	M	SD	M	SD	M	SD	M	SD
BASELINE	Lungs	-0.87	0.36	-0.5	0.25	-0.66	0.89	-1.66	0.24	-0.6	0.24	-0.83	0.14
	Heart	0.12	0.33	-0.5	0.25	0.16	0.13	0	0	-0.2	0.96	-0.16	0.13
	Spine	-1.12	0.6	0	1	-0.83	0.47	0.33	0.55	-1.2	0.16	-1	0
LOW-STRETCH	Lungs	-0.5	1.25	-1.5	0.25	-1.5	0.91	-1.66	0.24	-1.2	0.56	-0.33	1.55
	Heart	-0.62	0.74	-1	1	-1	0.33	-1.33	0.23	-0.8	1.36	0	0.66
	Spine	-2.12	0.85	-2	0	-2	1	-1.33	0.89	-1.8	2.16	-2.66	0.25
HIGH-STRETCH	Lungs	-2.12	0.38	-2.5	0.25	-2.83	0.15	-2	0.66	-2.8	0.16	-2	0.5
	Heart	-1	0.5	0	1	0.33	0.22	0.66	0.22	-0.4	0.64	0	1.33
	Spine	0.62	0.24	0	0	0.83	0.97	1	0	0	0	1	0.33

Table 4.4: Results of experiment 2 comparing the enhanced images with the film

analysis effectiveness?

The results of the comparison session are listed in Table 4.4 in terms of mean and standard deviation of selected rankings (between -3 and $+3$) for each image, each transformation and each of the three features: lungs, heart, spine when compared to the film.

The visibility of the lungs is slightly less clear in the baseline image than in the analog film. The heart is seen as slightly less clear to slightly more clear in the baseline image. The spine is often judged as being slightly less clear to less clear in the baseline image than in the analog film. The low-range stretching does not really improve these results for the lungs or the heart and definitely degrades them for the spine. However, the high-range stretching, compared to the film, sometimes improves the visibility of the heart and often the visibility of the spine.

These comparisons confirm the observation that the baseline image is a fairly "good" first overview and is in general close to the analog film. In some cases, the enhanced images also improve the visibility of features as compared with the analog film.

4.6 Experiment 3: Reverse mode transformations

4.6.1 Objective

The objective of the third experiment is to evaluate the usefulness of viewing radiographs in the reverse mode. The questions to be answered are the following ones:

- Is a reverse mode facility useful?
- What is the best image in the reverse mode?

4.6.2 Transformations and Method

The transformations of the first experiment are reversed (Fig. 4.7). The black areas were transformed into white ones and the white areas into black ones without changing the contrast. The same test procedure as in the first experiment is then applied. Eight radiologists participated in these tests.

4.6.3 Results

The results of this experiment are listed in Table 4. They show for each image and each physician the reversed transformation rated as "best".

	RAD1	RAD2	EM1	EM2	ICU1	ICU2
RADIOLOGISTS						
1	RTRUNC	RTRUNC	RTRUNC	RSQRT	RLLL	RTRUNC
2	RLLL	RTRUNC	RTRUNC	RSQRT	RLLL	RTRUNC
3	RLLL	RX2	RMID	RLLL	RTRUNC	RMID
4	RTRUNC	RTRUNC	RLLL	RSQRT	RTRUNC	RTRUNC
5	RTRUNC	RTRUNC	RTRUNC	RLLL	RLLL	RTRUNC
6	MID	RTRUNC	RTRUNC	RSQRT	RLLL	RLLL
7	MID	RTRUNC	RTRUNC	RLLL	RTRUNC	RTRUNC
8	RTRUNC	RX2	RTRUNC	RLLL	RTRUNC	RTRUNC

Table 4.5: Results of experiment 2 comparing the enhanced images with the film

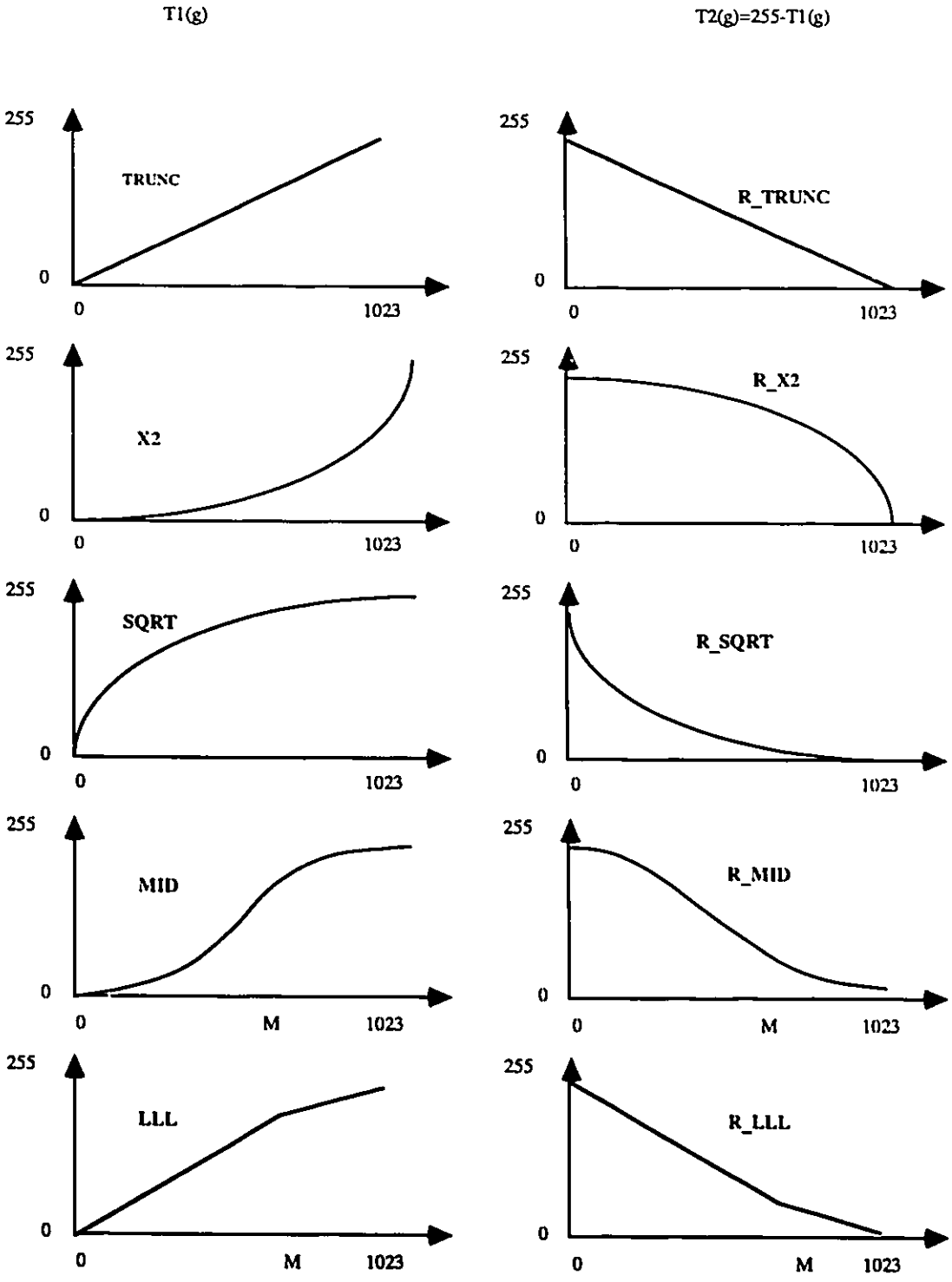

Figure 4.7: Reverse mode transformations

Is a reverse mode transformation useful?

All the physicians agreed that viewing images in the reverse mode could improve the visibility of certain areas and the detection of certain features.

What is the best image to be displayed in the reverse mode?

Table 4.5 shows that there is a high degree of concurrence in the radiologists'preferences regarding the aspect of a baseline image in the reverse mode. However these baseline images in the positive mode do not correspond to reversing the negative selected baseline images. The preferred images in the reverse mode are the reversed truncation (RTRUNC) in 54% of the cases and the reversed piecewise linear function (RLLL) in 29% of the cases. Contrary to experiment 1, the results are almost similar from one image to another and correspond either to leave the image unchanged or to stretch the low-range of grey levels. The smaller disparities between preferences for each image may be attributed to the unusual aspect of reverse mode images and the physicians' lack of practice in discriminating features in these images.

The best images in the reverse mode do not correspond in general to simply reversing the best baseline images in the usual positive mode.

4.7 Summary

Our approach to context-dependent enhancements attempts to match the three phases involved in viewing a radiograph : getting a global impression, analysing the objects and the local features, and focussing on the image perturbations. In this chapter, we reported on enhancements to support the two first phases in the case of chest radiographs. In addition, results on the applicability of grey level reversal transformations have also been reported.

It appears that the baseline view judged as giving the "best" global impression is

an image which provides in priority satisfactory visibility in the lung field. However enhancements which yield "best" baseline images are difficult to deduce when the original images are of poor quality. When the original images are of good quality, the concensus appears to be enhancements in the high-range or mean-range.

Global adaptive grey-scale manipulations yield a global change which is the result of an enhancement focussed on a part of the radiograph. They are useful as secondary images to support the analysis of the objects and of the local features in the image, in particular the spine, the inside of the lungs and of the heart. In terms of visibility of the lungs, the heart and the spine, we get close results to the analog film in using one or the other transformations including the one which yields the baseline image. This would suggest an implementation with preset enhancements for these areas under the user control.

The last experiment asserts the uselfulness of viewing radiographs in the reverse mode. However it appears that a good image in the reverse mode does not necessarily correspond to the reversal of the baseline image in the usual mode. In general the preferred images correspond to reversing the simple truncation function. Implementing a reverse mode facility requires the knowledge of the appropriate 8 bits to 8 bits remapping which transforms the baseline image in the usual mode to the desired one in the reverse mode.

Chapter 5

Subjective Evaluation of Local Enhancements

5.1 Introduction

In the case of chest radiographs, a global enhancement is more likely to yield an image of overall "good" visual quality, rather than an image of "optimal" quality for all the different areas in the image. As seen in the previous chapter, an image globally enhanced results from trade-offs and priorities in the appearance of different areas. Therefore, a global enhancement cannot support optimally the third phase involved in viewing a radiograph, namely the focal attention and scrutiny of the image perturbations (see Section 2-3-4). To support this phase, we propose to use the potential of local enhancements which will better highlight the areas of interest.

Our interest is particularly focussed on how to highlight specific pathologies since such an approach is more likely to be helpful for diagnosing these pathologies. Our ultimate goal would be automatic, content-dependent, local enhancement. Therefore, we first have to determine the viewing requirements for local pathological features and the enhancement techniques which meet these requirements.

In this chapter, we report on a user evaluation trial of local enhancements for specific pathologies, namely pulmonary nodule, pneumothorax, enlargement of paratracheal lymph node, interstitial lung disease and air bronchogram. We first present our objectives and method. We then explain how the trial was carried out. In the last section, we report the results of this trial.

5.2 Objectives

The objectives of the subjective evaluation tests of local enhancements were as follows:

1. Determine the efficiency of common enhancement techniques when they are applied to localized pathologies in images.

2. Determine which enhancements perform the best for specific pathologies.

3. Indirectly acquire knowledge regarding, for each pathology, what has to be enhanced so that the radiologist can improve his reading.

5.3 Material and Method

The hardware components used to prepare this experiment have been presented in Section 2.6. The software was written in the "C" programming language and run under the SCO Xenix 386 operating system.

The organization of the tests was separated into four parts: (i) selection of radiographs, (ii) extraction and recording of the windows of interest on the digitized radiographs, (iii) preparation of the "enhanced" windows, (iv) subjective testing.

The films, which were selected, contained the following pathologies: pulmonory nodule, pneumothorax, enlargement of paratracheal lymph nodes, interstitial lung disease and air bronchogram. They were extracted from teaching records, thus providing an archetypical sample of pathologies. In particular, examples were chosen where the pathological

problems are difficult to analyse on the original films. Then a radiologist selected the windows of interest on the digitized images, i.e. the windows surrounding the pathological problems.

5.4 Data Preparation

5.4.1 Method

The enhanced windows were prepared in advance so that they could be rapidly displayed. A header file contained the window coordinates, the name of the original image together with a list of the techniques used. All the enhancements or any single enhancement could be called up and displayed. The original window was also available as a window for display and comparison.

5.4.2 Enhanced Windows Creation

The enhancement techniques used are the same as those introduced in Chapter 3 and differ only in that they are applied locally. We recall these briefly here and indicate the various settings used for the parameters. We will use the same notations as in Section 3.3. The digitized chest images are of size 1200×1000 with 8 bits per pixel so that the range of grey levels is $G = [0, 255]$. In the following description of the methods, g denotes the original grey level and g' the transformed grey level.

The first technique is *windowing*, expressed as:

$$g' = \frac{(g'_{max} - g'_{min})}{(g_{max} - g_{min})}(g - g_{min}) + g'_{min} \tag{5.1}$$

g_{min} and g_{max} are computed from the unprocessed window data. We set (g'_{min}, g'_{max}) to $(0, 255)$ and $(30, 225)$. This last range is chosen to cope with the non-linearities of the display at extreme intensity values. In effect, details appear less clearly in very dark or very bright areas.

The second technique is *statistical differencing*:

$$g' = \frac{\sigma_{new}}{\sigma_{old}}(g - \overline{g}_{old}) + \overline{g}_{new} \tag{5.2}$$

where $\overline{g}_{old}$ and σ_{old} are known. We set $\overline{g}_{new}$, the new mean value, to 127 as the perceptibility of small contrast differences is greater in the middle range of intensities than in the extreme ranges, σ_{new} is set to a value two to four times that of σ_{old} in order to increase the contrast.

The third technique is a *polynomial remapping* :

$$g' = T(g) = Ag^3 + Bg^2 + Cg + D \tag{5.3}$$

where the coefficients are obtained from the following initial conditions:

$$g'_{min} = T(g_{min}),\ g'_{max} = T(g_{max}),\ s = T'(g_c),\ v = T(g_c).$$

g_{min} and g_{max} are known, (g'_{min}, g'_{max}) is set to $(0, 255)$, g_c is chosen either as the mean or the median of the window, the slope s at g_c is taken greater than 1, and v is set to 127.

The fourth technique is *histogram equalization*:

$$g' = (g'_{max} - g'_{min})cd(g) + g'_{min}, \tag{5.4}$$

where $cd(.)$ is the cumulative distribution function of the original histogram and (g'_{min}, g'_{max}) is set to $(0, 255)$ or $(30, 225)$ for the same reasons as equation 5.1.

The fifth contrast technique is *histogram hyperbolization*:

$$g' = (g'_{min} + c)\left(\frac{g'_{max} + c}{g'_{min} + c}\right)^{cd(g)} - c \tag{5.5}$$

where $cd(.)$ is the cumulative distribution function of the original histogram, (g'_{min}, g'_{max}) is set to $(0, 255)$ and c is function of the slope at 0 of the hyperbolized density function (see Section 3.4).

Three spatial techniques for edge enhancement were also tested: the first two are variations on unsharp masking and the third on edge detector:

(a) A *simple unsharp masking* expressed as :

$$g'(x,y) = c(g(x,y) - \overline{g}(x,y)) + \overline{g}(x,y) \tag{5.6}$$

where $\overline{g}(x,y)$ is constant over the entire window and set to the local mean. The value of the gain c varies between 1 and 5.

(b) A 5×5 *unsharp mask*:

$$g'(x,y) = c(g(x,y) - \overline{g}_{5,5}(x,y)) + \overline{g}_{5,5}(x,y) \tag{5.7}$$

where $\overline{g}_{5,5}(x,y)$ is a low-pass filtered window computed with an averaging mask of size 5×5. The value of the gain c varies between 1 and 10.

(c) As an edge detector, we use a *Sobel operator*:

$$g'(x,y) = c(g(x,y) * W(x,y)), \tag{5.8}$$

where $*$ is the convolution operator and $W(x,y)$ the Sobel mask (see Section.). The gain c is set to 5 so as to amplify the image signal.

5.5 Subjective Testing

5.5.1 Materials

The selected images represented 5 pathological groups characterizing 16 different cases decomposed as follows:

- four cases of pulmonary nodules of which two are located over the ribs,one over the heart and one partly over the rib and partly over the lung tissue,
- three cases of pneumothoraces, one is vertically oriented in the right lung, one horizontaly oriented at the left lung apex, and one horizontaly oriented at the right diaphragm border,

- two cases of air bronchograms, one in the upper part of the left lung and one in the lower part of the left lung,
- six cases of interstitial lung diseases, of which three are extracted from the right lung and three from the left lung and,
- one case of enlargement of paratracheal lymph nodes.

5.5.2 Procedure

The experimenter controlled completely the running of the tests so that the radiologist had only to concentrate on what was displayed on the screen.

To start the test for a given case, the original digitized image was first displayed and its preselected window appeared on the screen. This allowed the radiologist to locate the pathology in its original context. Then, the previously prepared enhanced windows appeared side by side on a black background. The radiologist was asked to rate the visibility of the pathologic feature for each window on a scale from -2 to 2 where -2 was 'not at all clear' and $+2$ was 'very clear'. The radiologist was then asked to rate in decreasing order the three preferred enhanced windows. Comments were encouraged on what the enhancement should be accomplishing and how well the objective was met. In the case where all the enhanced windows could not be displayed on the same screen, they were decomposed into two groups which were displayed in turn. The three first preferences of each were eventually redisplayed for a final selection of the overall preferred windows. This same procedure was repeated for each pathology.

5.6 Results

5.6.1 Introduction

Two radiologists participated in the tests. We judged this number sufficient to convey general guidelines for the local enhancements. The results are based on responses from the questionnaire used during the tests. They are both quantitative and qualitative.

Fig. 5.1 and Fig. 5.2 show two of the images used in the tests set: on the left with the window of interest surrounding the pathology, and on the right, the proposed enhanced windows for this pathology.

The results are summarized in Figures 5.3 and 5.4. Fig. 5.3 gives for each group of pathologies the ranking of the three preferred windows. They are referred to by the name of the enhancement technique from which they are derived. The abbreviations used in these two figures are explained in Fig. 5.5. We attributed a decreasing number of points to the first (3), second (2) and third choices (1), and calculated for each enhancement the total number of points by adding the contribution of each instance of a pathology. The three enhancements retained in the final ranking were those with the highest number of points. In Fig. 5.4, we show in graphic form the average ratings received by enhancement and pathology. In the case where there were several occurrences of the same enhancement technique with different settings of the parameters, we retained the setting which yielded the best numerical rating.

5.6.2 General Observations

From the results summarized in Fig. 5.4, we can draw the following remarks:

- For each pathology, there is always a processed window which brings out the pathological features better than the unprocessed window (original) does. This clearly demonstrates the potential of local enhancement techniques.

Figure 5.1: Air bronchogram

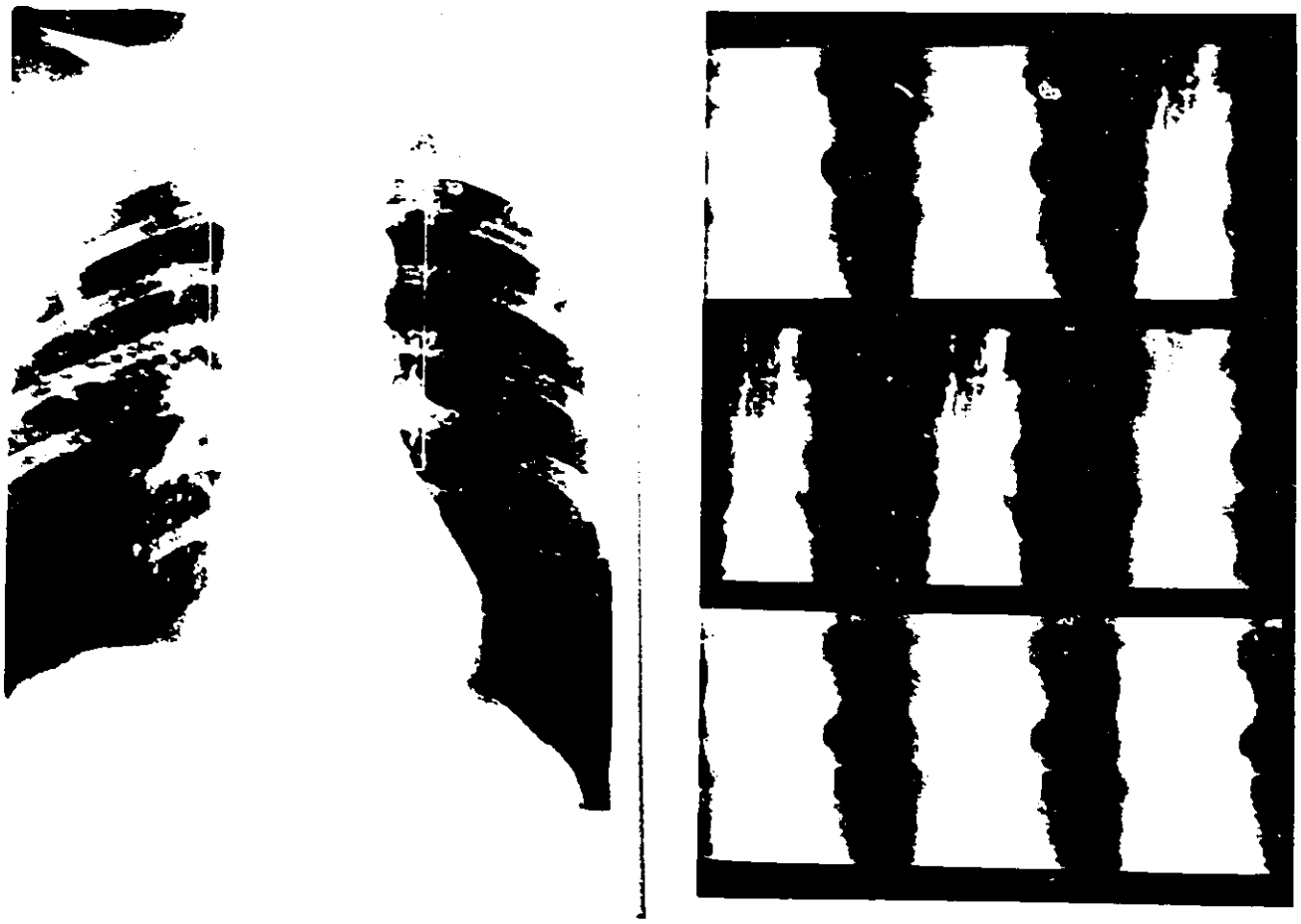

Figure 5.2: Enlargement of paratracheal lymph nodes

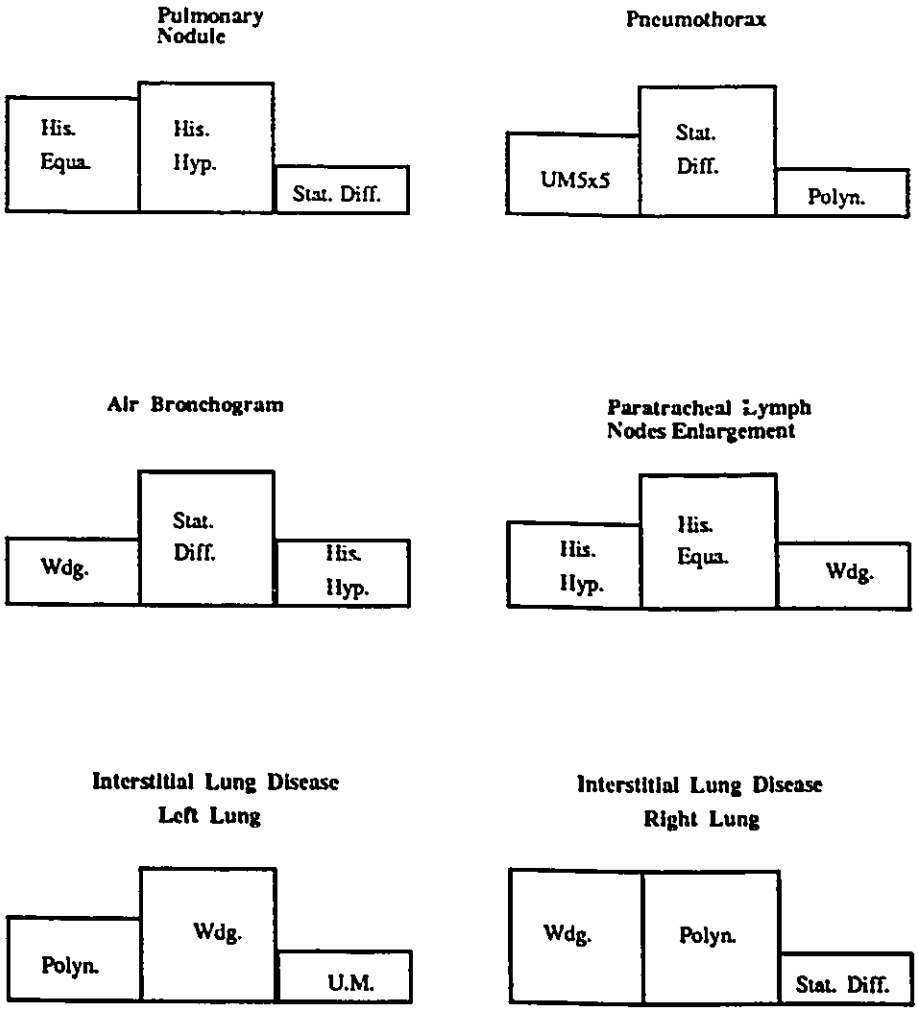

Figure 5.3: Preferences for each group of pathologies

Figure 5.4: Numerical rating for each enhancement technique

Abbreviation	Enhancement
Orig.	Original (unprocessed)
Wdg.	Windowing
Stat.Diff.	Statistical Differencing
Polyn.	3d degree polynomial transform
His. Equa.	Histogram Equalization
His.Hyp.	Histogram Hyperbolization
U.M.	Simple unsharp masking
U.M.5x5	Unsharp masking with a 5x5 window
Sob.	Sobel Detector

Figure 5.5: Abbreviations for the enhancements

- The performance of spatial enhancement techniques (*Simple Unsharp Masking*, 5×5 *Unsharp Masking* , *Sobel Detector*) is in general poor compared with contrast techniques (*Windowing*, *Statistical Differencing*, *Polynomial Transform*, *Histogram Equalization*, *Histogram Hyperbolization*).

- In particular, the Sobel transform was constantly rated last.

- The rated efficiency of an enhancement technique varies with the pathology.

- *Statistical Differencing* is the best overall technique.

5.6.3 Preferred enhancement by pathology

In this section, we analyse the results for each group of pathologies and summarize the comments given by the radiologists during the tests as to what feature they expected to see improved. We also give our suggestions on what enhancement technique to retain and

to refine.

Pulmonary Nodules

The average size of the windows containing the pulmonary nodules is 75×85. Two of these nodules are located completely under a rib, one is over the lung tissue and another one extends both over the lung tissue and under the rib. Those nodules are scrutinized for their *delimitations* and *content*. In particular, the radiologists want to see if there are inner signs of *calcification*.

As shown in Fig 5.3, the three preferred enhancements for the nodules are *Histogram Hyperbolization*, *Histogram Equalization*, *Statistical Differencing*. The first two techniques increase the contrast drastically which implies an over-enhancement of the nodule itself, independently of its context. *Statistical Differencing* along with *Polynomial Transform*, *Windowing* and *Simple Unsharp Masking* were preferred for the fourth nodule (which extended over the lung tissue and under the rib), as high contrast techniques resulted in a blurring of the margins of the nodule. For this case, the techniques preferred increase the contrast while keeping the details both inside and outside the nodule. These remarks are reflected by the numerical rating for each technique (Fig. 5.4). The good ranking of *Statistical Differencing* can be explained as a trade-off between high contrast and retention of fine details.

In terms of numerical rating, *Histogram Equalization* and *Histogram Hyperbolization* yielded rather close results, as the appearance of the respective enhanced windows were close. We favour the technique with the easiest parameters to set: *Histogram Equalization*. Hence, we propose to keep two kind of techniques for the enhancement of nodules:

- *Histogram Equalization* with $g'_{min} = 0$ and $g'_{max} = 255$. This enhancement provides high contrast to bring out large isolated nodules.

- *Statistical Differencing* with $\overline{g}_{new} = 127, \sigma_{new} = c\sigma_{old}$ where $c = 3$ or 4. This method increases the contrast to a lower extent but retains the fine details and so is useful in perceiving tiny diffuse nodules as well as in providing a natural appearance in the window.

Pneumothorax

A pneumothorax appears as a thin line around the margin of a lung resulting from free air in the pleural space. We had three cases of pneumothoraces of which two were very subtle. The sizes of the surrounding windows of interest are respectively (49 × 381), (182 × 79) and (230 × 109). The objective of the enhancement is to bring out the pneumothorax line.

On average, the preferred enhancements are *Statistical Differencing*, 5 × 5 *Unsharp Masking* and *Polynomial Transform*. *Statistical Differencing* and *Polynomial Transform* both increase smoothly the contrast thus keeping a natural aspect in the processed windows. *Histogram Equalization* and *Histogram Hyperbolization* did not bring out well the pneumothorax line and also gave windows which are too "black and white", and therefore, unpleasant for the eye. For the pneumothorax located at the apex of the left lung, only 5 × 5 *Unsharp Masking* succeeds in bringing out the line. In terms of average numerical ratings (Fig 5.4) , the four best enhancements are *Statistical Differencing*, *Polynomial Transform* and *Windowing*.

Combining the preferences with the numerical ratings, we can suggest the following techniques for the enhancement of pneumothoraces:

- *Statistical Differencing* with $\overline{g}_{new} = 127$ or $\overline{g}_{new} = \overline{g}_{old}$, $\sigma_{new} = c\sigma_{old}$ where $c = 2$ to 5. This method provides a smooth increase in contrast which is likely to be suited for most of the pneumothorax cases. We favour it over *Polynomial Transform* as its parameters are easier to set.

- *Windowing* with $g'_{min} = 30$ and $g'_{max} = 225$ as a technique which maintains a good visibility inside the window.

- 5×5 *Unsharp Masking* with a gain value of 10 as a last resort when no contrast technique can bring out the pneumothorax.

Air bronchogram

The size of the two windows surrounding the air bronchograms are respectively (224×282) and (196×301). They are located in the upper part and the lower part of the left lung.

To diagnosis an air bronchogram, one has to visualize clearly air filled bronchi within lung parenchyma. These bronchi do not show up in normal lungs. When the lung is white, the visualization of bronchi allows diagnosis of *air-space consolidation*, i.e. the filling of pulmonary air spaces with abnormal material, such as inflammatory exudate in pneumonia or blood in pulmonary hemorrhage. This is the reason why the preferred enhancements (Fig. 5.3) are those that increase the contrast, namely *Statistical Differencing*, *Windowing* and *Histogram Hyperbolization* with an inclination for a medium and smooth increase as obtained with *Statistical Differencing* and *Windowing*. The average numerical ratings (Fig. 5.4) reflects these preferences and also show the good ranking of *Histogram Equalization* along with *Histogram Hyperbolization*.

To bring out an air bronchogram, we, therefore, suggest the following enhancements:

- *Statistical Differencing* with $\overline{g}_{new} = 127$ or $127 \leq \overline{g}_{new} \leq mean$, $\sigma_{new} = c\sigma_{old}$ where $c = 2$ or 3, for a smooth increase in contrast, which brings out the pathology and provide a good visibility in the window.

- *Histogram Equalization* with $g'_{min} = 0$ and $g'_{max} = 255$ for greater contrast enhancement than in *Statistical Differencing*. This is preferred to *Histogram Hyperbolization*, which yields approximately the same results and has more parameters to set.

Enlargement of Paratracheal Lymph Nodes

The selected window of size (253 x 356) is located in the upper part of the mediastinum, centered on the trachea and the mainstem bronchi. The radiologists want to visualize, in particular, the paratracheal stripe which delimits the wall of the trachea from the adjacent soft tissues. When this stripe is lost because of a soft tissue mass, this is likely to be due to an enlargement of the paratracheal lymph nodes.

The preferred enhancements are *Histogram Equalization* and *Histogram Hyperbolization* as in effect, high contrast allows to visualize clearly the tracheal air column and the paratracheal region. The preferences are also consistent with the numerical rating.

For such window selections, we suggest to apply:

- *Histogram Equalization* either with $g'_{min} = 0$ and $g'_{max} = 255$ or $g'_{min} = 30$ and $g'_{max} = 225$ which gives a high contrast enhancement.

Interstitial Lung Disease

For each image, the selected windows of average size (215 x 460) include the outer third of the right and left lungs. Interstitial lung disease typically results in blurring the vascular pattern of the lungs, and gives rise to extra lines and/or nodules which are often best distinguished in the outer third of the lungs. The radiologists look for enhancements which accentuate the nodules, which sharpen the lines and bring out the blood vessels.

Their preferred enhancements (Fig. 5.3) for both the right and left lung are those that give medium contrast and deblur the disease features, as provided by *Windowing*, *Polynomial Transform*, *Statistical Differencing*. In particular, these techniques provide sharper lines at the lung periphery. *Simple Unsharp Masking* was also retained as a good technique for its capability of sharpening the lines while maintaining sufficient contrast

inside the lungs. However, this was sometimes at the expense of loosing the definition of the thoracic cavity border. High contrast techniques, such as *Histogram Equalization* and *Histogram Hyperbolization*, tend to destroy parts of the window content and to wash out other parts. The preferences are consistent with the average numerical ratings (Fig. 5.4) which further indicates that an enhancement for Interstitial Lung Disease corresponds also to a good appearance of the window because of the diffuse characteristic of the disease.

For interstitial lung disease, we therefore suggest to retain the following enhancements:

- *Windowing* with $g'_{min} = 0$ and $g'_{max} = 255$, for a medium increase in contrast which retains and accentuate most of the details.

- *Polynomial Transform* with $g_c = \overline{g}$, $s \simeq 2$ and $v = 180$ which can sometimes provide sharper lines than in *Windowing*.

5.6.4 Variabilities of the ratings

In Fig. 5.6, we show how the three (unordered) preferences of the two radiologists match over the entire sample (16). In all 16 cases, there is at least one common preference, in 7 cases two common preferences and in 6 cases all three are common. In Fig. 5.7, we show now how the two first (unordered) preferences match over the entire sample. In 14 cases, there is at least one common preference and in 5 cases the two first preferences are common. These results demonstrate the similarity between the two radiologists'preferences. Fig. 5.8 reflects the variabilities on the numerical ratings between the two radiologists. In 81% of the cases, their ratings are the same or differ by one value only.

This consistency in the choices of the two radiologists increases our confidence in the results of the limited subjective testing.

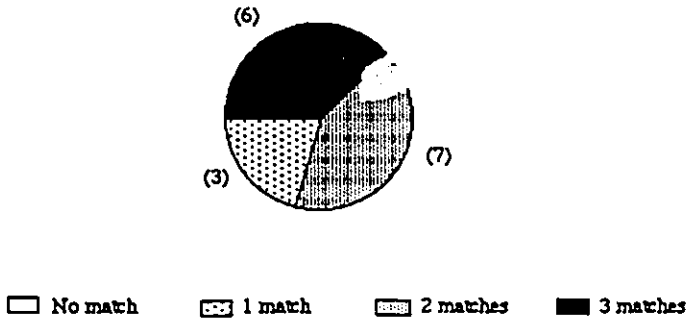

Figure 5.6: Matching in the three first preferences between the radiologists

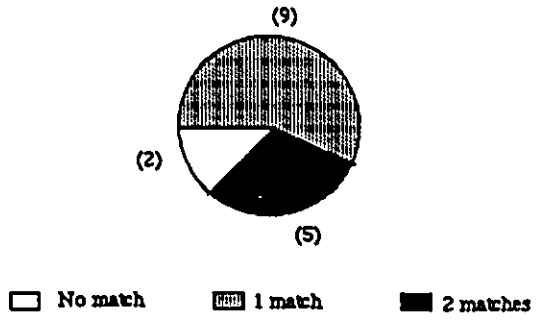

Figure 5.7: Matching in the two first preferences between the radiologists

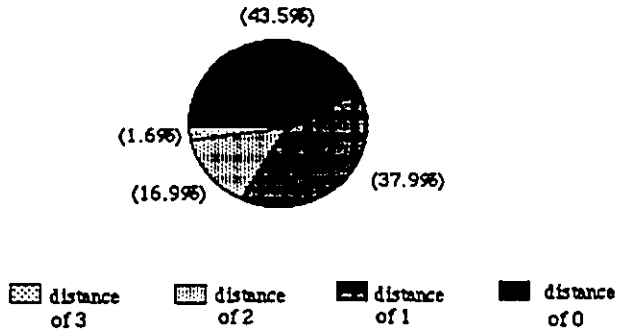

Figure 5.8: Matching in the numerical ratings between the radiologists

5.7 Summary

In this chapter, we reported on enhancements to support the last phase involved in viewing a radiograph, namely focussing on the image perturbation, and we presented the results of a subjective user evaluation trial.

The main objectives of this trial were to determine the efficiency of common enhancement techniques for specific pathologies and acquire knowledge regarding how the pathology could be optimally highlighted. We particularly focussed our interest on the following pathologies: pulmomary nodule, pneumothorax, enlargement of paratracheal node, interstitial lung disease and air bronchogram. We had one to six digitized radiographs for each pathological case.

It appeared that the rated efficiency of an enhancement technique varies with the pathology. For each pathology, we described the features that the radiologist required to be highlighted, and we reported on the enhancements with their parameter settings which the closest achieved these goals. Thus, we propose *Histogram Equalization* and *Statistical Differencing* to enhance pulmonary nodules, *Statistical Differencing, Windowing*

and 5 × 5 *Unsharp Masking* to bring out pneumothoraces, *Statistical Differencing* and *Histogram Equalization* to highlight air bronchograms, *Histogram Equalization* to highlight paratracheal lymph nodes and *Windowing* and *Polynomial Transform* to enhance interstitial lung disease.

Although only two radiologists evaluated the enhancements, their choices were often the same. This makes us confident about the results of these limited tests.

Chapter 6

Parametric histogram specification of digitized chest radiographs

6.1 Introduction

In this chapter, we investigate the use of *global histogram specification* for chest images, in which a given image is transformed so that its histogram matches the histogram of some ideal image. This technique belongs to the context-free class, however we shall show below that it can be made to adapt to the context of the image, while at the same time not suffering from the problems of context-sensitive techniques. In our preliminary study, the pre-specified histogram is one corresponding to a "good" quality chest radiograph, as chosen by radiologists. However instead of using the histogram directly, the original chest image is processed to yield parametric characteristics of a good chest image. This is required as chest radiographs differ greatly from one another because of the patient's anatomy, the possible pathology and the radiograph acquisition technique. The direct histogram specification technique does not take into account these inherent characterisitics of the chest radiograph, some of which should not be altered.

Our approach called *parametric histogram specification (PHS)* thus considers *parametric models* for the characterisation of the grey levels distribution of chest radiographs rather than only the histogram values. The first objective, therefore, is to specify a

parametric model for an "ideal" chest radiograph. This model stresses the fundamental similarity between chest radiographs as it assumes that the difference can be expressed by the specification of a few parameters.

In other words, our main hypothesis is that chest radiographs belong to a general class, which can be specified by a family of distributions. To define the appropriate model corresponding to this family of distributions, we rely on results obtained from a previous study [PLESSIS, 89] as well as on results published by MacAdams et al [MCADAMS, 86]. Both studies assert the intrinsic bimodal nature of the distribution of chest radiographs. Consequently, we looked for a bimodal model which could characterize the corresponding distribution. This model must be parametric to take into account the inherent characteristics of each chest image. As a suitable model, we chose to consider a mixture of two normal distributions. Such a model is completely described by its parameters and these parameters must be related to some characteristics of the radiograph, namely the subject's anatomy or possible overall pathology and the film acquisiton method.

It is clear that we must concentrate on those parameters which are related to the film acquisition method as these often impinge upon image quality. Given a "poor" quality image, enhancement is now a two stage process. We first attempt to fit a bimodal distribution to the histogram. Those parameters corresponding to the subjects'anatomy and pathology are retained and combined with the parameters that correspond to an ideal image, in effect correcting for poor film acquisition.

In the following section, we first report on methods for characterizing chest radiographs and on the use of direct histogram specification. In Section 6.3, we present our bimodal parametric model and estimation methods for parameter extraction. In Section 6.4, we then show how this can be applied for image enhancement. This follows in Section 6.5 with pictorial results.

6.2 Characterization of digitized chest radiographs in term of histogram

6.2.1 Histograms of digitized chest radiographs

In Fig. 6.1, we present grey level histograms of digitized chest radiographs. These radiographs were digitized with a laser scanner manufactured by Konica which provides images of size 2000×2430 pixels with 1024 grey levels. For display requirements, the digitized images were low-pass filtered and sub-sampled to 1000×1200 pixels and the number of grey levels was also reduced from 1024 to 256. From now on, we shall use indifferently the terms "digitized chest radiograph" and "chest image". The shape of the histograms varies considerably and depends upon factors such as film quality, subject anatomy and pathologic conditions.

6.2.2 Histograms of good quality chest images

In a previous study [PLESSIS, 89] transformations were applied to chest images of different quality and the resulting images were judged by physicians. An image was rated of "good" quality if it had satisfactory overall visibility for diagnosis. In particular, when the original radiograph is already of good quality, the appearance of the digitized image must be at least as good as the corresponding radiograph. In Fig. 6.2, we show two examples of histograms of chest images which were rated as "good quality".

6.2.3 Histogram specification

In the continuous case, the transformation to be applied to a given distribution so as to yield a second distribution is found as follows [HALL, 79]: Let X_1 and X_2 be two continuous random variables. If X_1 has a cumulative distribution function F_1 and X_2 has a cumulative distribution function F_2, the random variables $F_1(X_1)$ and $F_2(X_2)$ both have a uniform distribution. Hence $F_2^{-1}(F_1(X_1))$ has the same distribution as X_2. In the

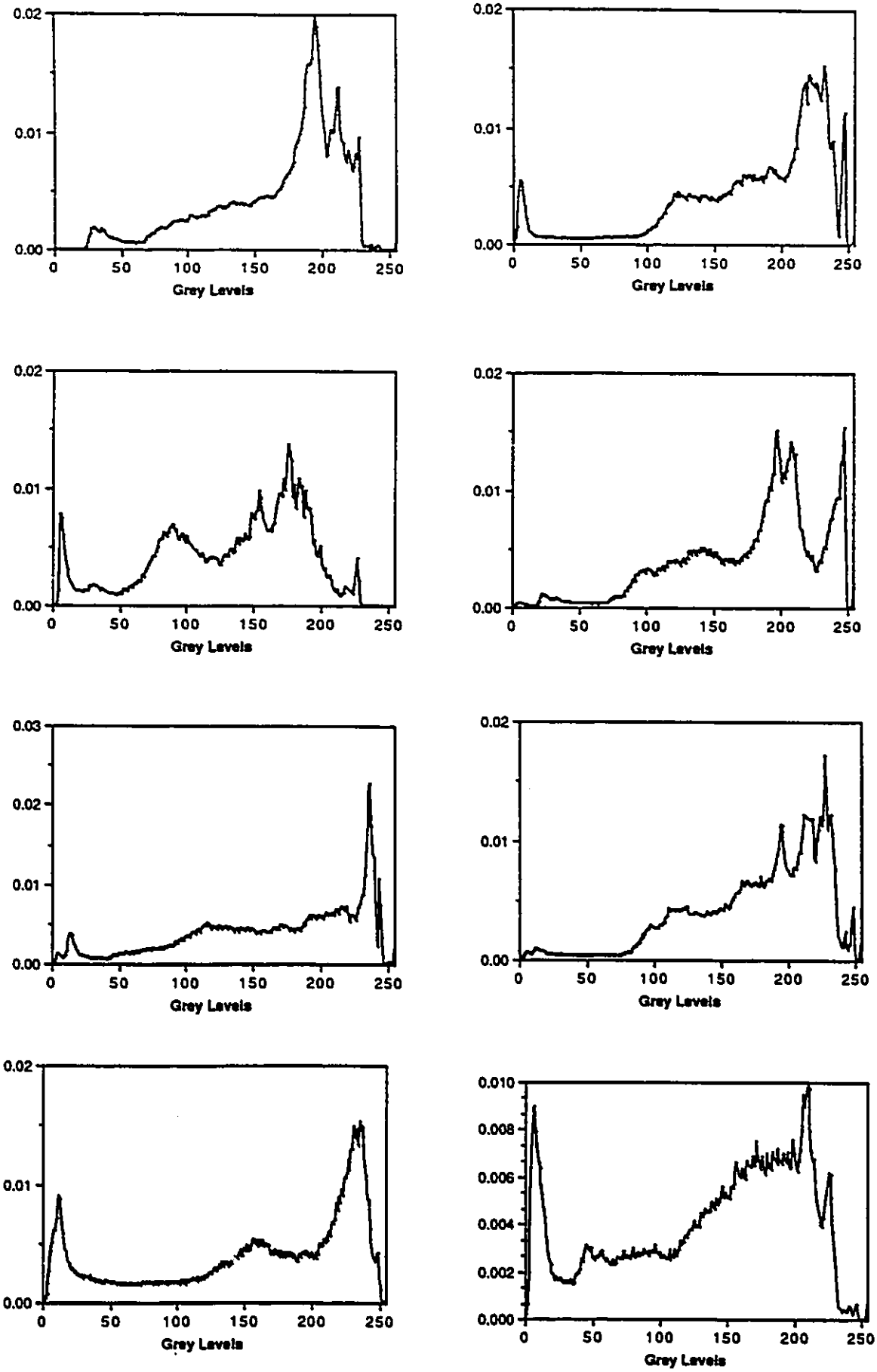

Figure 6.1: Grey level histograms of digitized chest radiographs

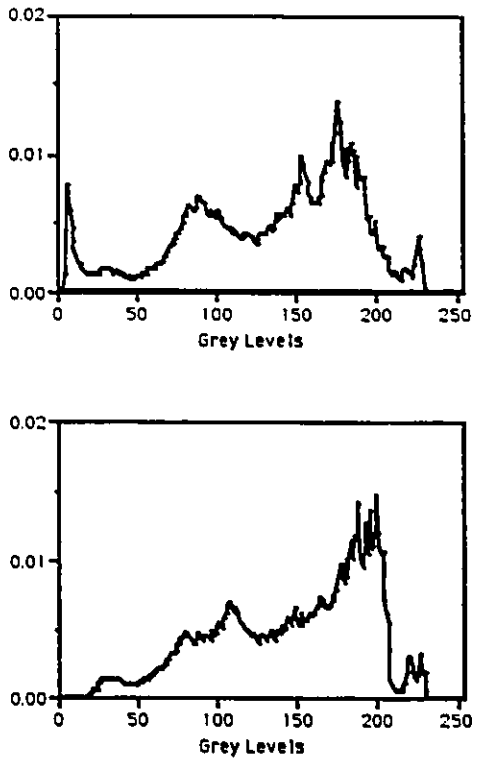

Figure 6.2: Grey level distribution of good quality chest images

discrete case, this result does not hold exactly, however for a large enough number of steps, the approximation is quite acceptable. We first estimate the cumulative distributions F_1, F_2 from the original histogram and the desired histogram, respectively. The new grey levels are then obtained by applying the transformation $F_2^{-1} \circ F_1$ on the original grey levels.

In Fig. 6.3, we show two images and in Fig. 6.4, we show their corresponding histogram. The first image has been rated as "good quality", whereas the second image has been rated as "poor". In Fig. 6.5, we show the result of using histogram specification, i.e. the histogram of the "poor" quality image is transformed so as to approximate that of the "good" quality image. The result of such a transformation is rather spurious as the inner parts of both lungs are completely "destroyed" and their periphery is blurred.

Rather than specifying just to a histogram of an arbitrary image, we may specify an ideal histogram derived by an averaging of the histograms of a number of "good" images, in essence trying to reduce the noise. Fig. 6.6 gives an example of an averaged histogram. Fig. 6.7 shows the result of using the average histogram as the basis for histogram specification. We see that an important part of the lungs is still blackened and their periphery is blurred resulting in a loss of details.

6.2.4 Search for a model

From the results of *direct histogram specification*, we can deduce that there are inherent characteristics in each chest image which should not be altered. Our goal is to parametrically model a chest histogram in order to later propose a chest-adapted histogram specification.

We want first to take advantage of the fact that all chest radiographs have similar features and belong to a general class. The class definition relies on the hypothesis that chest radiographs grey level distributions always belong to a special family of distributions

Figure 6.3: Image of "good" quality (first one) and image of "poor" quality

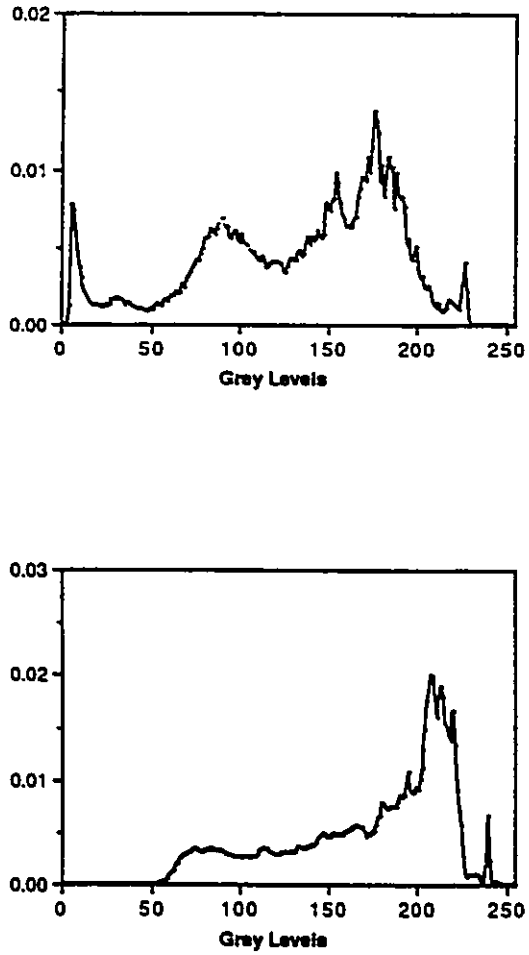

Figure 6.4: Histograms of the previous "good" and "poor" quality images

Figure 6.5: Result of histogram specification

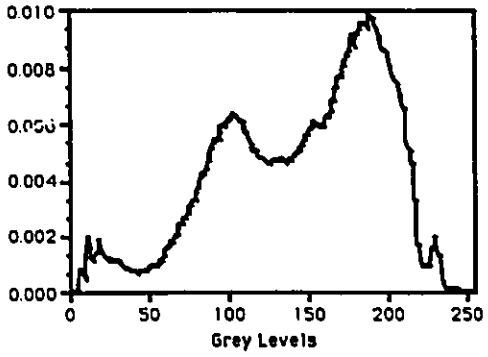

Figure 6.6: Averaged histogram

Figure 6.7: Result of histogram specification with the averaged histogram

because of their general shape. This family and, as a consequence, the general class have to be specified by an appropriate parametric model.

Let us consider the first histogram in Fig. 6.2. We can disregard the two extreme peaks which correspond to the background influence, we are thus left with essentially a bimodal histogram. MacAdams et al [MCADAMS, 86] have also analysed chest radiograph histograms and have concluded that the thoracic cavity, which contains the significant information in a chest image, shows an histogram which is bimodal with significant lung field-mediastinum histogram peak separation.

These observations suggest that the distribution of grey levels in a chest image can be satisfactorily described by an appropriate mixture of two normal distributions where the first normal distribution represents the lung field and the second one represents the mediastinum and subdiaphragmatic areas. Furthermore, this restriction reduces the estimation

of the grey levels distribution to the one of a small number of parameters.

6.2.5 Interpretation of the model parameters

The mixture of two normal distributions is characterized by the following density:

$$f(x;\mu_1,\mu_2,\sigma_1,\sigma_2,p) = p.\varphi(x;\mu_1,\sigma_1) + (1-p).\varphi(x;\mu_2,\sigma_2)$$

where $\varphi(x;\mu,\sigma)$ is the one-dimensional normal density. It is completely described by the value of its five parameters: $\mu_1,\mu_2,\sigma_1,\sigma_2,p$, where we assume that each parameter has a meaning in terms of information content. In the case of the chest image, the histogram clearly provides spatial information and this property has been used to choose the model. Namely, the first uni-modal distribution can be related to the grey level distribution of the lung field, and the second one can be related to the grey level distribution of the mediastinum and sub-diaphragmatic areas. As a consequence, μ_1 (μ_2) represents the brightness of the lung field (mediastinum and sub-diaphragmatic areas) and σ_1 (σ_2) is an indication of the contrast. Thus $\mu_1,\mu_2,\sigma_1,\sigma_2$ depend upon factors determined by the film technical quality. The weights of each distribution, p and $1-p$, are more representative of the extent of the lung field versus the mediastinum and sub-diaphragmatic areas in the image, in other words, the patient's anatomy. We note that in the case where the subject shows an overall pathology in the lung field, this also influences the value of p.

6.3 Parametric modeling of the distribution of grey levels in chest radiographs

6.3.1 Introduction

Parametric models for the distribution of grey level values of chest images have been proposed in literature. For example, Cocklin et al [COCKLIN, 83], use a parametric model based on the Rayleigh distribution: $f(x) = x\exp(-x^2/2)$ to compensate for the

fact that, in general, the distribution of grey levels of chest images is heavily weighted towards the high intensity values. Their model is specified with the following parameters:

x^0_{min}, x^0_{max}, the minimum and maximum grey level values in the observed histogram,

x_{min}, the minimum grey level value in the parametric histogram,

a, some constant,

and the truncated distribution is expressed as follows:

$$f(x) = \frac{b}{a^2} \times (x - x_{min}) \exp\left(-(x - x_{min})^2/2a^2\right)$$

where

$$b = 1/(1 - \exp\left(-(x^0_{max} - x^0_{min})^2/2a^2\right))$$

Tubbs [TUBBS, 87] has proposed a general model for a "variable shape probability density function" which follows a Beta-distribution. This parametric model is given by:

$$f(x) = \frac{(x - x^0_{min})^{\alpha-1}(x^0_{max} - x)^{\beta-1}}{B(\alpha,\beta)(x^0_{max} - x^0_{min})^{\alpha+\beta-1}}$$

for $x^0_{min} \leq x \leq x^0_{max}$ and

$$B(\alpha,\beta) = \int_0^1 u^{\alpha-1}(1-u)^{\beta-1} du$$

This latter model has the drawback of being too general for chest radiographs and the parameters α and β are difficult to identify.

Both models consider a uni-modal distribution rather than a bimodal one which does not correspond to the actual histograms of chest radiographs We find it more appropriate to propose a bimodal parametric model based on the mixture of two normal distributions. In the following, we will make more precise the definition of the model and propose different ways to estimate its parameters.

6.3.2 Model

The classical mixture problem consists in specifying the distribution for observations which come from n different sub-populations, each with a known density. In many situations, the density function of each sub-population, $f_i(.), i = 1, \ldots, n$, has a parametric form, $f_i(./\theta_i)$, where θ_i represents the parameters of $f_i(.)$, and each sub-population has a probability p_i of being selected. Thus we have the following expression for the probability density function of the mixture:

$$f(x) = \sum_{i=1}^{n} p_i f_i(x/\theta_i) \tag{6.1}$$

where

$$p_i > 0 \text{ and } \sum_{i=1}^{n} p_i = 1$$

.

In our case, we can distinguish two different sub-populations, one corresponding to the lung field and one corresponding to the mediastinum and sub-diaphragmatic areas. We assume that both sub-populations follow the same normal distribution with different parameters, $N(\mu_1, \sigma_1^2)$ and $N(\mu_2, \sigma_2^2)$ respectively. Hence, the density of the mixture of the two normal distributions with proportion p and $1 - p$ respectively is expressed as follows:

$$f(x) = \frac{1}{\sqrt{2\pi}}(p\frac{\exp(-(x-\mu_1)^2/2\sigma_1^2)}{\sigma_1} + (1-p)\frac{\exp(-(x-\mu_2)^2/2\sigma_2^2)}{\sigma_2}) \tag{6.2}$$

where $0 \leq p \leq 1$. The first moment of the mixture, i.e. the mean, is given by:

$$m_1 = E(X) = p\mu_1 + (1-p)\mu_2 \tag{6.3}$$

The second moment is given by:

$$m_2 = E(X^2) = p(\sigma_1^2 + \mu_1^2) + (1-p)(\sigma_2^2 + \mu_2^2) \tag{6.4}$$

The third moment is obtained as follows:

$$m_3 = E(X^3) = p\mu_1(3\sigma_1^2 + \mu_1^2) + (1-p)\mu_2(3\sigma_2^2 + \mu_2^2) \qquad (6.5)$$

6.3.3 Estimation

General method

The problem of estimating the components of a normal mixture has been studied since Pearson (1894). However, unless one is ready to accept some restricted assumptions about the model, no closed form expression is available for estimating the parameters of the mixture. Furthermore, it appears that the classical method of the *maximum likelihood* cannot be applied in the case of a mixture of normal distributions, even if some approximative methods are available [TITTERINGTON, 85]. In effect, given a sample of N independent observations, the likelihood function which is given by,

$$L(p, \mu_1, \sigma_1, \mu_2, \sigma_2) = \prod_{i=1}^{N} f(x_i) = \prod_{i=1}^{N} [p f_1(x_i; \mu_1, \sigma_1) + (1-p) f_2(x_i; \mu_2, \sigma_2)]$$

can be bounded from below as,

$$L(p, \mu_1, \sigma_1, \mu_2, \sigma_2) \geq \frac{p}{\sigma_1} \exp((x_1 - \mu_1)^2/\sigma_1^2) \prod_{i=2}^{N} \frac{1-p}{\sigma_2} \exp((x_i - \mu_2)^2/\sigma_2^2)$$

since each term in the developed product is positive. If we set x_1 to μ_1 then when σ_1 tends toward 0, the likelihood tends toward ∞. Even if we agree upon boundaries on the variances, this method still requires extreme computations as well as any minimum distance estimation method of densities or of cumulative distribution functions. Consequently, we choose to use the alternative ***method of moments*** for the estimation [TITTERINGTON, 85], which we now describe.

Consider first a mixture of two normal distributions with density,

$$f(x; \mu_1, \mu_2, \sigma_1, \sigma_2, p) = p.\varphi(x; \mu_1, \sigma_1) + (1-p).\varphi(x; \mu_2, \sigma_2) \qquad (6.6)$$

where φ is the one-dimensional normal density and let $x_1, x_2, \ldots, x_n$ represent the sample values, i.e. the pixel values. The method of moments consists in equating the observed moments

$$M_r = \frac{1}{n}\sum_{i=1}^{n} x_i^r \qquad r = 1, \ldots, 5 \tag{6.7}$$

to the theoretical moments given by

$$m_r = \int x^r f(x)dx \qquad r = 1, \ldots, 5. \tag{6.8}$$

In the normal case, these moments are related to the parameters of the mixture by equation (6.3), (6.4) and (6.5).

We then obtain the following system of five non-linear simultaneous equations, which must be solved to give estimates of the five parameters in the mixture distribution, $\hat{\mu_1}, \hat{\mu_2}, \hat{\sigma_1}, \hat{\sigma_2}, \hat{p}$

$$\hat{p}\hat{\mu_1} + (1-\hat{p})\hat{\mu_2} = M_1$$

$$\hat{p}(\hat{\sigma_1}^2 + \hat{\mu_1}^2) + (1-\hat{p})(\hat{\sigma_2}^2 + \hat{\mu_2}^2) = M_2$$

$$\hat{p}(\hat{\mu_1}\hat{\sigma_1}^2 + \hat{\mu_1}^3) + (1-\hat{p})(\hat{\mu_2}\hat{\sigma_2}^2 + \hat{\mu_2}^3) = M_3$$

$$\hat{p}(3\hat{\sigma_1}^4 + 6\hat{\sigma_1}^2\hat{\mu_1}^2 + \hat{\mu_1}^4) + (1-\hat{p})(3\hat{\sigma_2}^4 + 6\hat{\sigma_2}^2\hat{\mu_2}^2 + \hat{\mu_2}^4) = M_4$$

$$\hat{p}(15\hat{\sigma_1}^4\hat{\mu_1} + 10\hat{\sigma_1}^2\hat{\mu_1}^3 + \hat{\mu_1}^5) + (1-\hat{p})(15\hat{\sigma_2}^4\hat{\mu_2} + 10\hat{\sigma_2}^2\hat{\mu_2}^3 + \hat{\mu_2}^5) = M_5$$

By some tedious algebra, these equations may be reduced to a ninth degree polynomial from which the root(s) have to be extracted [TITTERINGTON, 85].

A first approximation

When constraints are placed on some of the parameters, the computation may be considerably simplified. We introduce here some simplifying assumptions based upon the observation of the actual empirical histogram.

First, for "good" quality images, we have observed that (1) the two modes are relatively far apart; (2) as a consequence, this allows us to assume that each mode of the mixture corresponds to the mean of one of the normal distributions. Let $mode_1$ and $mode_2$ be the two modes of the mixture, the estimates for μ_1 and μ_2 are given by

$$\hat{\mu_1} = mode_1 \tag{6.9}$$

$$\hat{\mu_2} = mode_2 \tag{6.10}$$

Let K be the number of grey levels and let $p(i)$ be the frequency of occurence of grey level i. Given equation (6.7) which estimates the first and second moments and which can also be expressed in function of the $p(i)'s$,

$$M_1 = \sum_{i=0}^{K} ip(i) \tag{6.11}$$

and

$$M_2 = \sum_{i=0}^{K} i^2 p(i), \tag{6.12}$$

we have the following equations for the estimate of the remaining parameters $\hat{p}, \hat{\sigma_1}, \hat{\sigma_2}$:

$$M_1 = \hat{p}\hat{\mu_1} + (1-\hat{p})\hat{\mu_2} \tag{6.13}$$

$$M_2 = \hat{p}(\hat{\sigma_1}^2 + \hat{\mu_1}^2) + (1-\hat{p})(\hat{\sigma_2}^2 + \hat{\mu_2}^2) \tag{6.14}$$

Furthermore, if $h_1 = p(mode_1)$ ($h_2 = p(mode_2)$) is the height of the empirical histogram at the first (second) mode, our assumptions imply that h_1 (h_2) is proportional to $\frac{\hat{p}}{\hat{\sigma_1}}$ ($\frac{1-\hat{p}}{\hat{\sigma_2}}$) and the proportionality coefficient is the same. Therefore,

$$\frac{h_1}{h_2} = \frac{\hat{p}}{1-\hat{p}} \frac{\hat{\sigma_2}}{\hat{\sigma_1}} \tag{6.15}$$

Equations (6.13), (6.14), (6.15) are then sufficient for the estimation of p, σ_1, σ_2.

A second approximation

Unfortunately, the previous crude assumptions are not necessarily satisfied for all chest images. Bad quality images, such as those taken with portable units, may have distributions with just one well defined mode (Fig. 6.8) or with two different modes which are close to one another (Fig. 6.9). However, one mode in the bright areas will always be pre-eminent which leads us to consider a less restrictive set of assumptions for estimating the parameters of the model.

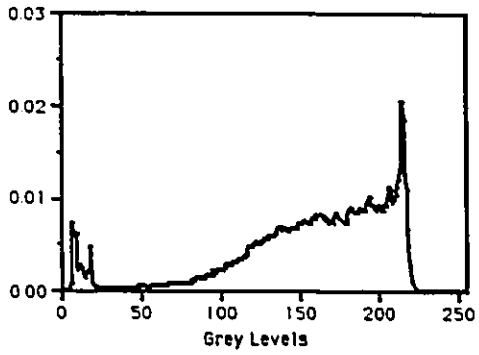

Figure 6.8: Distribution with one well defined mode

We will assume that (i) the main mode of the empirical histogram, $\hat{\mu_2}$, is a good approximation of the mean of the second normal distribution , μ_2, and (ii) the overlap due to the first distribution is neglectible at the point $\hat{\mu_2}$. Note that this is not the case for concentrated histograms such as the one in Fig.6.9. For such distributions, one will have to use the general method of moments (see 6.3.3). Under the assumptions (1) and (2), the height of the empirical histogram, $p(mode_2)$, is an acceptable estimator of $\frac{1-p}{\sqrt{2\pi}\sigma_2}$.

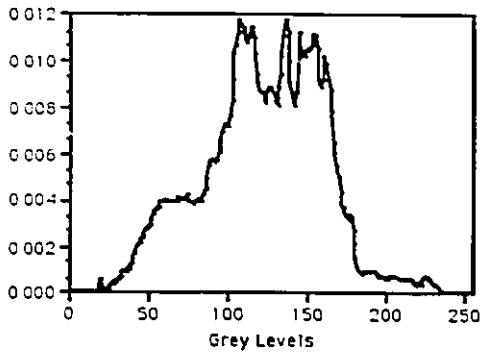

Figure 6.9: Distribution with modes close to one another

If we write, $p(mode_2) = \frac{h}{\sqrt{2\pi}}$, we have then the equality :

$$h = \frac{1 - \hat{p}}{\hat{\sigma}_2} \tag{6.16}$$

Using the estimator of the third moment (Eq. (6.7)) here expressed as a function of the $p(i)$'s:

$$M_3 = \sum_{i=0}^{K} i^3 p(i), \tag{6.17}$$

we get a third equation:

$$M_3 = \hat{p}\hat{\mu}_1(3\hat{\sigma}_1{}^2 + \hat{\mu}_1{}^2) + (1 - \hat{p})\hat{\mu}_2(3\hat{\sigma}_2{}^2 + \hat{\mu}_2{}^2) \tag{6.18}$$

We note that the following changes can be made:

(i) equation (6.13) yields $\hat{\mu}_1$ as a function of $\hat{p}$:

$$\hat{\mu}_1 = \frac{M_1 - (1 - \hat{p})\hat{\mu}_2}{\hat{p}} \tag{6.19}$$

(ii) equation (6.14) yields $\hat{\sigma}_1{}^2$ as a function of $\hat{p}$:

$$\hat{\sigma}_1{}^2 = \frac{1}{\hat{p}}[M_2 - \frac{(M_1 - (1 - \hat{p})\hat{\mu}_2)^2}{\hat{p}} - (1 - \hat{p})(\hat{\mu}_2{}^2 + (\frac{1 - \hat{p}}{h})^2)] \tag{6.20}$$

(iii) and equation (6.18) yields a 6-degree polynomial in $\hat{p}$:

$$A\hat{p}^6 + B\hat{p}^5 + C\hat{p}^4 + D\hat{p}^3 + E\hat{p}^2 + F\hat{p} + G = 0 \tag{6.21}$$

where

$$\begin{aligned}
A &= 3\hat{\mu_2} \\
B &= 3(M_1 - 5\hat{\mu_2}) \\
C &= 3(-3M_1 - 9\hat{\mu_2} + h^2\hat{\mu_2}^3) \\
D &= (3 + h^2\hat{\mu_2}^2)M_1 - 5\hat{\mu_2} - 3h^2\hat{\mu_2}^3 \\
E &= (3 - 9h^2\hat{\mu_2}^2)M_1 + h^2(M_2\hat{\mu_2} + 10\hat{\mu_2}^3 - M_3) \\
F &= h^2(M_1 - \hat{\mu_2})(M_2 - 6M_1\hat{\mu_2} + 6\hat{\mu_2}^2) \\
G &= -2h^2(M_1 - \hat{\mu_2})^3
\end{aligned}$$

We are only interested in the solutions between 0 and 1. Several cases may occur:

1. There is one solution $\hat{p}$ so that $0 \leq \hat{p} \leq 1$, then our model is completely parametrized.

2. There is no root $\hat{p}$ so that $0 \leq \hat{p} \leq 1$, then the estimation process will fail and the general method of moments has to be used instead.

3. There are several roots so that $0 \leq \hat{p} \leq 1$. In this case, we choose, among the roots making $\sigma_1^2 \geq 0$ the one closest to $1/2$.

Remark: These two methods are bound to be criticized from a statistical viewpoint as being too *ad hoc* and lacking of rigor. However, apart from the gain in computation time brought by these approximations, it is worth to note that the normal mixture modelization is still an approximation of the grey levels distribution. Therefore the use of theoretically more accurate statistical methods (e.g. the general method of moments) will not necessarily lead to a better approximation of the exact distribution.

6.4 Application to enhancements

6.4.1 Parametric Histogram Specification (PHS)

In PHS, the parameter, p, used in the bimodal model of the grey level distributions is assumed to convey the information about the patient's anatomy and disease.

Given a bad quality image, the enhancement by *PHS* is decomposed into two processing stages: (1) determining the parametrized bimodal model and keeping only the estimated weight $\hat{p}$, (2) applying the histogram specification with a parametrized model using $\hat{p}$ with the μ's and σ's derived from some "ideal" image. Thus, the processed image should now have the same characteristics as a good quality image while retaining the anatomical information content.

The determination of the parameters in the model is a three-step procedure described in Section 6.3.3. In the first step, we detect the two modes in the image histogram. In parallel, we compute the moments directly from the histogram as shown in equations (6.11) and (6.12). We can now use equations (6.9),(6.10),(6.13),(6.14) and (6.15) to determine the parameters.

The operator used to detect the modes of the histogram is a composite of a smoother, S_N, and a differentiator, D_n. S_N is obtained by averaging the histogram over a moving window of size N:

$$w_N(i) = 1/N, \frac{-(N-1)}{2} \leq i \leq \frac{N-1}{2}.$$

At each point, i, in the histogram where the first difference (approximating the first derivative) equals 0, D_n computes the sign of the first difference for the n previous points and the n following points. Point i is a local maxima if the first differences are positive for the n points before i and negative for the n points after i. When more than two local maxima are detected, we apply the two following rules: (1) discard the two peaks which have extreme positions (very dark or very bright grey levels), (2) among the remaining

maxima, choose the 2 heighest peaks. This assumes that the smoothing is efficient enough to transform close local maxima into a unique one.

The motivation to discard the peaks with extreme positions when they exist, is supported by the observation that they are not, in general, part of the significant information in the chest image but reflects more the influence of the background. This remark suggests also to compute the moments over a truncated histogram where the influence of the background is not taken into account. The percentage of background contribution is not known *a priori* but such values could be obtained statistically after having observed a broad collection of chest images.

In Fig. 6.10, we summarize the processing steps involved in *PIIS*.

6.4.2 The "ideal" model

As remarked in Section 6.2.2, an image is of "good" quality if it has a satisfactory overall visibility for diagnosis. Furthermore, when the film is already of good quality, the digitized image should be at least as good. It is clear that the ideal model should have the characteristics of "good" quality images, however one has to specify precisely these characteristics.

We first wanted to verify the stability of the inherent parameters as extracted from the bimodal model of "good" quality images. We selected a sample of 10 "good" quality films, without much variations in patients'anatomy. We then estimated the parameters $\mu_1, \mu_2, \sigma_1, \sigma_2$ and p for each image. The resulting average and standard deviation of the estimates are indicated in Table 6.4.2 for each parameter.

	μ_1	μ_2	σ_1	σ_2	p
average	105.33	188.88	32.3	18.2	0.5
standard deviation	11.18 (4.36%)	7.38 (2.88%)	5.62 (2.19%)	4.5 (1.75%)	0.08 (8%)

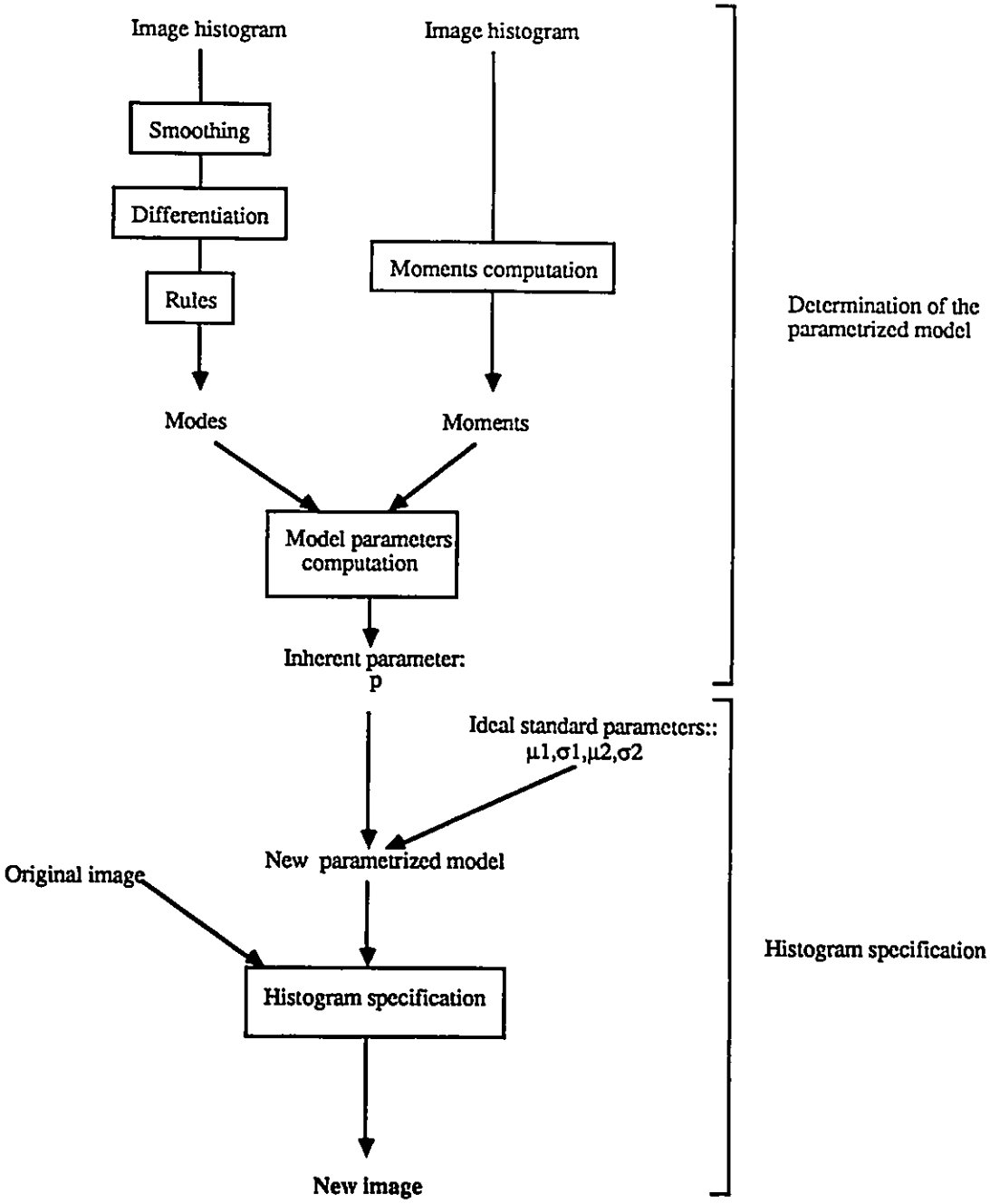

Figure 6.10: Adaptive Histogram Specification

As expected, the parameter p is the most variable of all five parameters which reflects its importance as an indicator of the variation in patients'anatomy. The parameters $\mu_1, \mu_2, \sigma_1, \sigma_2$ vary to a lesser extent, which is an indication of their general stability for "good" quality images.

In the results presented, we used the averaged estimates of the parameters to generate an "ideal" bimodal grey level distribution.

6.5 Results

6.5.1 Behaviour of the model

In Fig. 6.11, we show a number of histograms of chest images on which is superimposed the corresponding computed parametrized model. It is clear that the parametrized model fits reasonnably well to the histogram. We also note that the parametrized model of the averaged histogram of good quality images (Fig. 6.12) is very close to the parametrized model obtained by averaging the parameters of each single histogram. These results point out the robustness of the parameters estimation procedure despite the restrictive hypothesis made (see Section 6.3.3).

6.5.2 Pictorial results

The images presented in this section were selected by radiologists.

Application of PHS to "good" quality images

PHS is intended to improve the appearance of "poor" quality images, however, at the same time it should not alter the appearance of "good" quality ones. In Fig 6.13 and Fig 6.14, we show two good quality images (on the left hand side) and the result of applying *PHS* (on the right hand side). The processing has not altered the original images, which demonstrates its stability for "good" quality images.

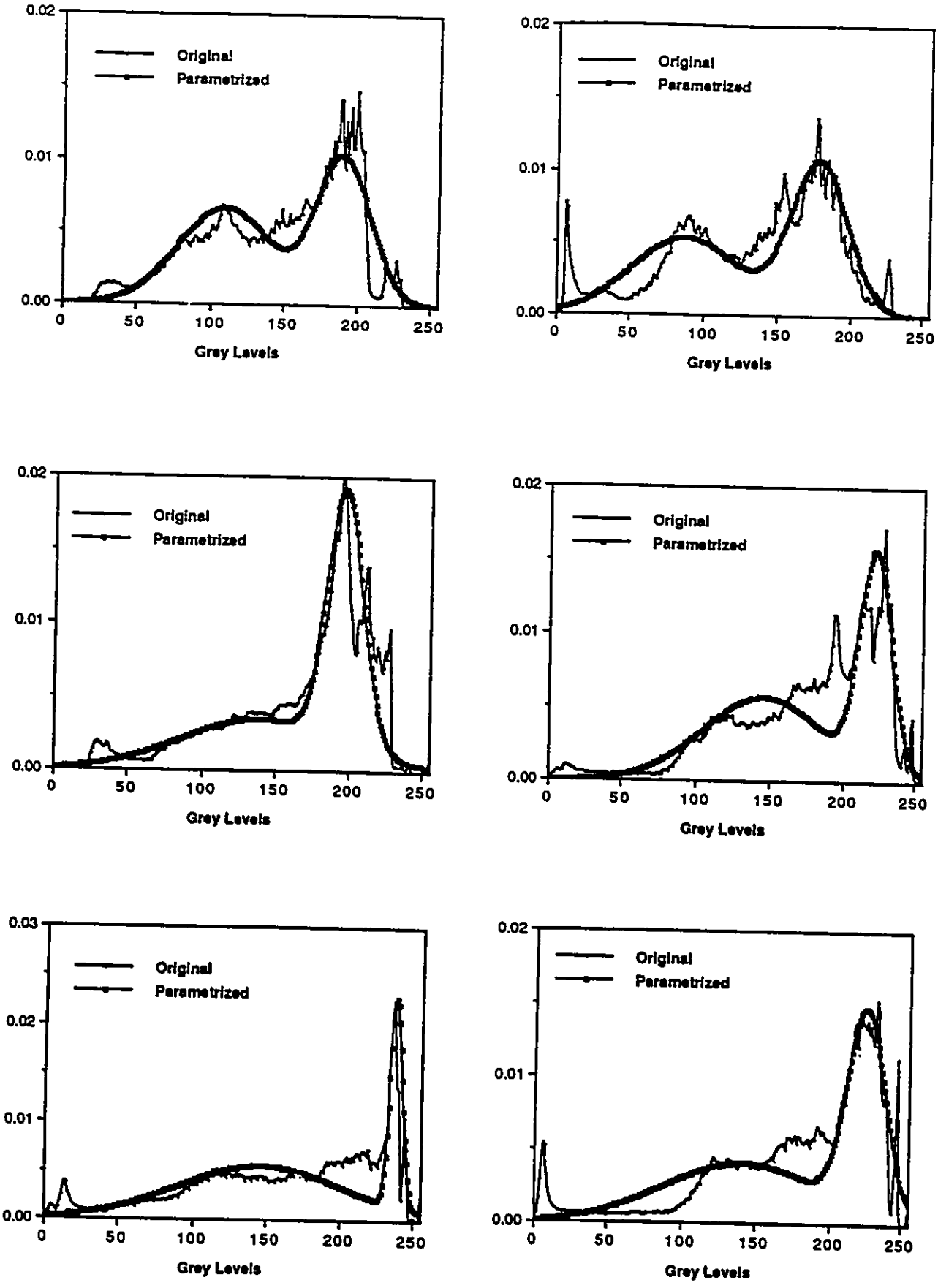

Figure 6.11: Histograms of chest images and their models

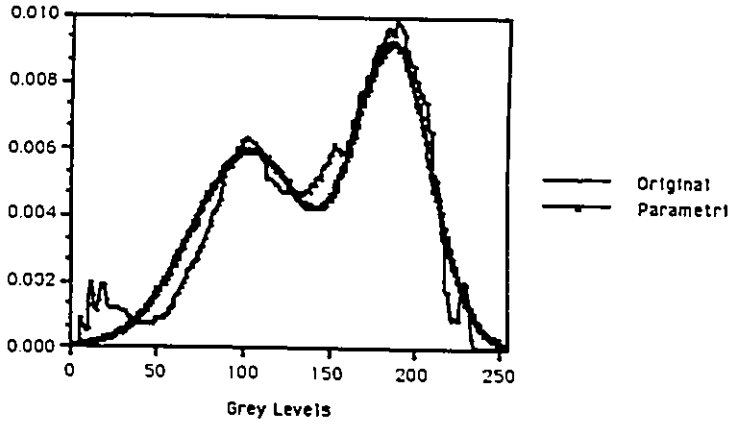

Figure 6.12: Average histogram of "good" quality images and its model

Variations of the parameter p

In *PHS*, the parameter p characterizes the patient's anatomy and is obtained from the parametrization of the histogram of the original image. In Fig. 6.15 and Fig. 6.16, we show the results of applying *PHS* to the first image of Fig.6.17 but using different values of p. The computed value of p in the original parametrization is 0.76 and results are shown corresponding to, respectively, from left to right in the first figure, $p = 0.2, p = 0.5$, and to $p = 0.8$ in the second figure. The perceived quality of the image increases as the value of p comes closer to the true value. The $p = 0.2$ image is completely washed out, in the $p = 0.5$ image, the appearance of the right lung has been improved but the quality of the left lung is still poor, finally, in the $p = 0.8$ image, details appear in both right and left lungs as well as in the mediastinum.

The results demonstrate that the parameter p is an important inherent descriptor which should not be altered.

Application of PHS to "poor" quality images

We now present the results of applying *PHS* to "poor" quality images. For each case,

Figure 6.13: Application of PHS to a "good" quality image

Figure 6.14: Application of PHS to a "good" quality image

Figure 6.15: Variations of the parameter p

Figure 6.16: Variations of the parameter p

we show the original image on the left side and the processed image on the right side.

In Fig. 6.17, the original image presents a right lung which is completely black and a left lung which is completely white and from which the mediastinum cannot be distinguished. After applying *PHS* details in both lungs and in the mediastinum are now revealed. Also, the air bronchogram is now clearly visible in the upper part of the left lung. The spine is better defined as well.

The original image shown in Fig. 6.18 is too " black and white". *PHS* reduces this wide dynamic range and as a result reveals more details in the lungs and in the heart. The spine also becomes more visible.

The original image in Fig. 6.19 presents blurred lung details, due to a diffuse lung disease, and is poorly contrasted in the mediastinum. The processed image sharpens the details in the lungs, especially in the lower half of the lungs. The trachea is completely apparent and the mediastinum is more contrasted, particularly in the hilum and the heart areas.

Fig. 6.20 shows the result of applying *PHS* to the same image as in Fig. 6.3. Compared to the original image, some details are lost at the apex of the lungs but the mediastinum clearly gains in visibility (see the trachea, the hilum, the heart). The air bronchogram in the lowest half of the left lung is also clearly distinguishable. The results should be compared with histogram specification shown in the second image of Fig. 6.3. The lungs are not completely "destroyed" as in the direct histogram specification technique.

The original image in Fig. 6.21 is too "white" and too blurred. *PHS* yields a more appealing image with good contrast both in the lungs and mediastinum. Details are sharpened in the lungs and more information appears in the heart and the spine.

The original image in Fig. 6.22 is too "white" in the right lung and in the mediastinum. *PHS* increases the contrast in the right lung and in the mediastinum while maintaining the same visibility through the left lung.

This series of examples demonstrate the applicability of *PHS* for improving "poor" quality chest images.

6.6 Summary

In this chapter, we have presented a parametric histogram specification technique, called *PHS*, for the enhancement of digitized chest radiographs of "poor" quality.

The goal is to obtain an image presenting the characteristics of "good" quality images, while maintaining the inherent characteristics of the original image, in particular those which touch on the patient's anatomy and pathology. We have proposed a bimodal parametric model to characterise the grey levels distribution of chest radiographs, which is based on a mixture of two normal distributions. The parameters of the model are related to the following characteristics of the radiograph: the subject's anatomy, the possible overall pathology and the film acquisition method. Given a "poor" quality image, enhancement through *PHS* consists in specifying the model of the final grey level distribution by combining the parameters which correspond to the subject's anatomy and pathology with the film acquisition parameters of an "ideal" image.

We have shown graphic results on how the proposed bimodal parametric model fits to the histogram of a chest image. We have also presented pictorial results of *PHS*. In particular, we have shown that *PHS* maintains the appearance of "good" quality images and clearly improves the aspect of "poor" quality images.

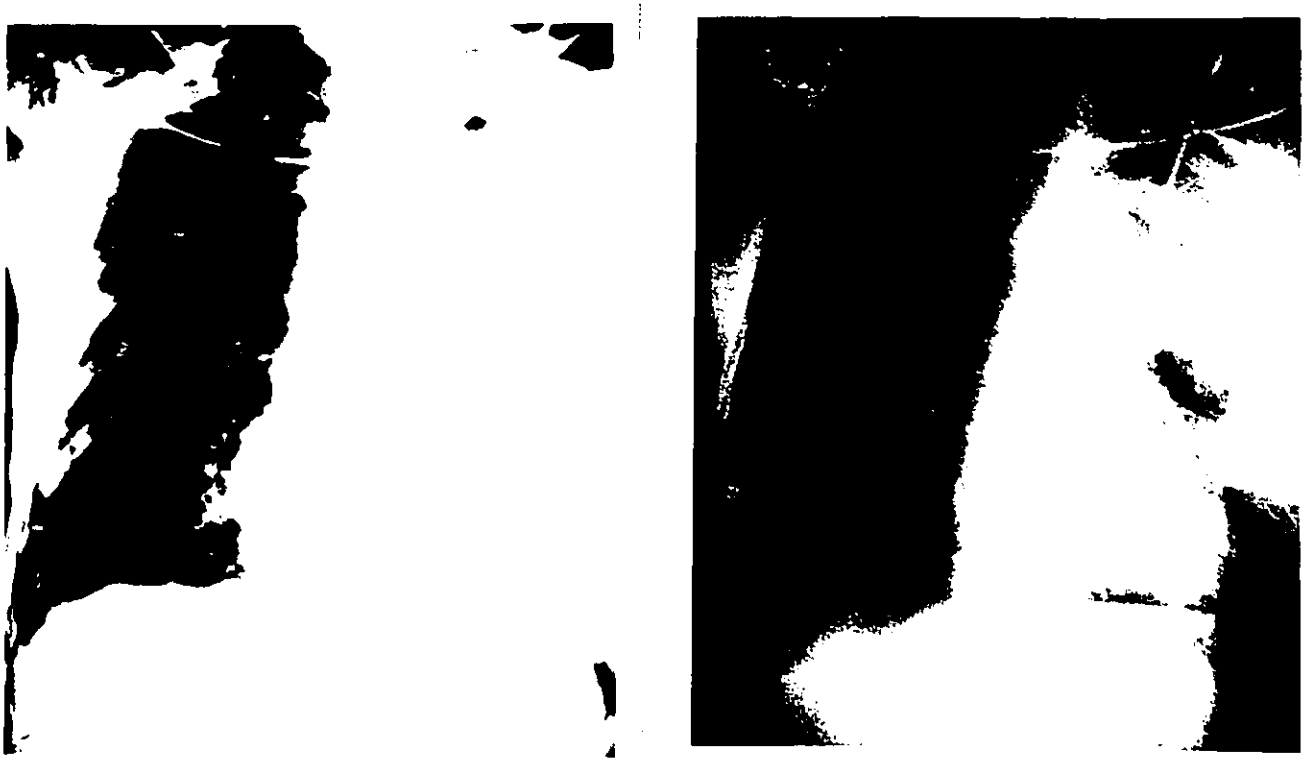

Figure 6.17:

Figure 6.18:

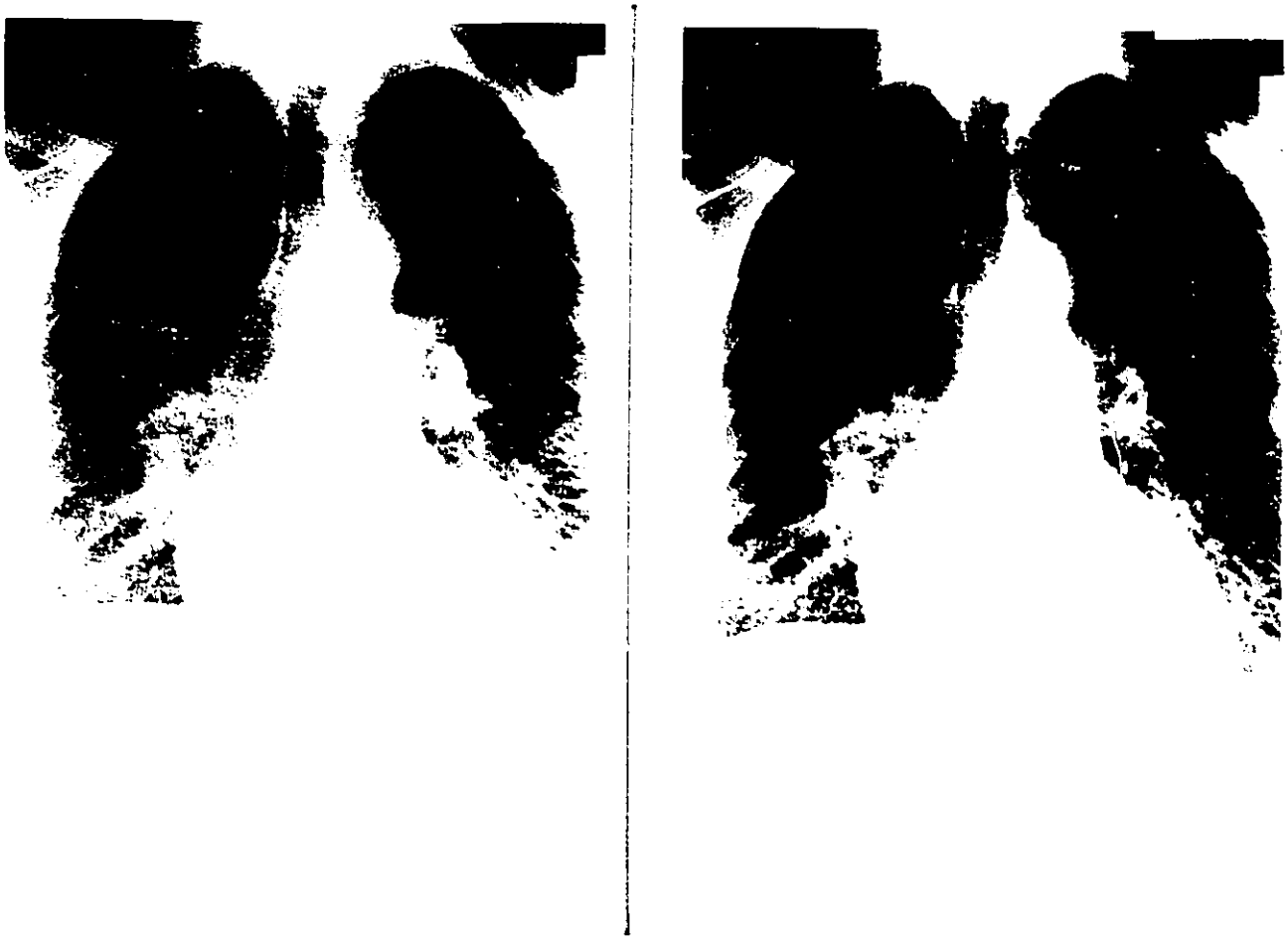

Figure 6.19:

Figure 6.20: the first image is the original image, the second image is the processed one

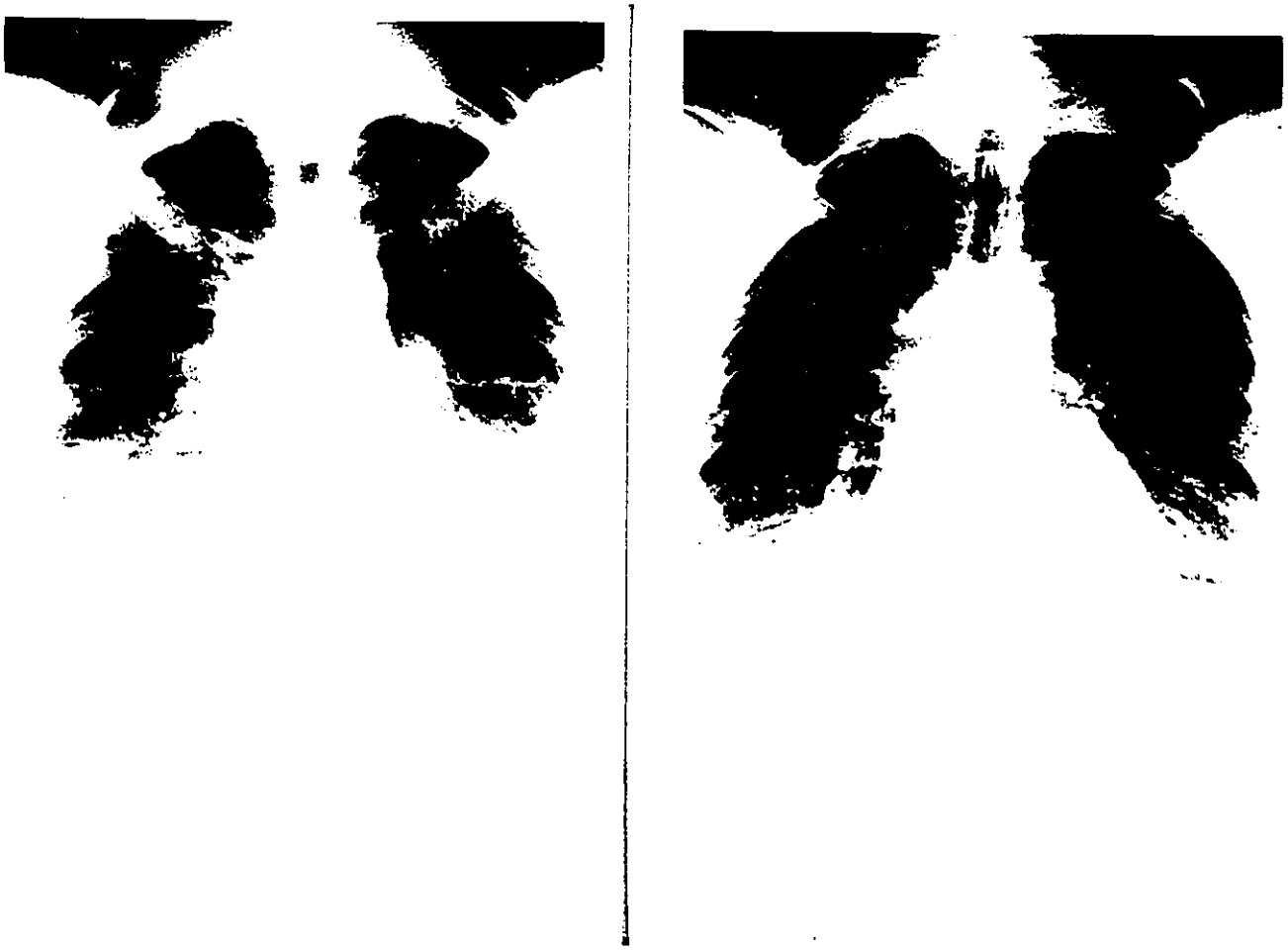

Figure 6.21:

Figure 6.22:

Chapter 7

Summary and suggestions for further research

In this thesis, we have investigated the viewing requirements involved in the review of a chest radiograph and determined the relevance of various enhancement techniques to meet these requirements. These objectives are motivated by the necessity to achieve the ultimate goal of automatic context-dependent enhancement for digitized radiographs.

Our approach to context-dependent enhancements attempts to match the three phases involved in viewing a radiograph: getting a global impression, analyzing the objects and the local features and focussing on image perturbations. From a first series of tests on the evaluation of images quality, we deduced that:

1. In the case of "good" quality films, an enhancement which stretches the high range or middle range of the grey scale provides a good baseline view close to the analog film, but in the case of "poor" quality films, an enhancement which provides an acceptable baseline view is more difficult to deduce.

2. Global adaptive enhancements based on piecewise-linear transformations of the grey-scale are useful as secondary images to support the analysis of objects and local features.

3. Reverse mode transforms are useful and give better results when they are context-

dependent.

In a second series of tests, radiologists evaluated the application of various local enhancements to highlight specific pathologies. The results demonstrate that the enhancements should be context-dependent as their applicability varies with the pathology. It appears that, in general, techniques which modify the contrast (e.g. *Statistical Differencing*, *Histogram Equalization*) are preferred and that spatial technique are rejected. We have described the preferred enhancement with their parameters settings for each group of pathology.

We have also introduced a new enhancement technique, *Parametric HIstogram Specification (PHS)*, which aims at providing a good baseline view for "poor" quality images. The basis of this technique is on the characterization of the histogram of digitized chest radiographs as a bimodal parametric model, specifically a mixture of two normal distributions. The parameters of the model are related to different characteristics of the chest image: the patient's anatomy, the possible overall pathology, the film acquisition technique. *PHS* then consists in specifying an estimated final histogram for the "poor" quality image which has the characteristics of a "good" image and maintains at the same time its inherent characteristics (anatomy, pathology). We have also proposed a simplified method of estimation of the parameters and showed that it works satisfactorily. Experimental results on a number of images show that,

1. the appearance of "good" quality is not altered,

2. the appearance of "poor" quality images is definitely improved.

We can suggest the following topics for further research:

1. A wider experiment with a large number of images is needed to refine the transforms (high and middle grey level range stretching) which provide baseline views for "good" quality chest radiographs.

2. The medical value of applying *PHS* on "poor" quality chest images needs to be evaluated in a clinical trial.

3. Further work on context-dependent enhancements is required in the case of reverse display of chest images.

4. Context-dependent enhancement should be extended to digitized radiographs which image other part of the body.

References

[BLUME, 87] Blume H., Kamiya K., "Auto-ranging and normalization versus histogram modifications for automatic image processing of digital radiographs," *SPIE Medical Imaging*, vol. 767, pp. 371-383, 1987.

[BRODY,84] Brody W.R., *Digital Radiography.* New York: Raven Press, 1984.

[BROGDON, 83] Brogdon B.G., Kelsey C.A., Mosley R.A., "Factors affecting detection of pulmonary lesions," *Radiol. Clin. North. Am.*, vol. 21, pp. 633-654, 1983.

[COCKLIN, 82] Cocklin M., Kaye G., Kerr I., Lams P., "Image enhancement of chest radiographs using local statistical information," *Proc. 1st International Symposium on Medical Imaging and Image Interpretation*, Berlin, Octobre 1982, 82-85.

[COCKLIN, 82a] Cocklin M., Kaye G., Kerr I., Lams P., "Digital enhancement of pneumothoraces," *Proc. 1st International Symposium on Medical Imaging and Image Interpretation*, Berlin, Octobre 1982; 82-85.

[COCKLIN, 83] Cocklin M.L., Gourlay A.R., Jackson P.H., Kaye G., Kerr I.H., Lams P.,"Digital processing of chest radiograph," *Images Vis. Comput.*, pp. 1-67, 1983.

[COOMBS, 70] Coombs C.H., Dawes R.M., Tversky A., *Mathematical psychology: an elementary introduction.*, Englewood Cliffs, NJ: Prentice Hall, 1970.

[DAPONTE, 88] DaPonte J.S., Martin D.F., "Enhancement of chest radiographs with gradient operators," *IEEE Trans. on Medical Imaging* vol.7,2, pp. 109-117, June 1988.

[FAHNESTOCK, 83] Fahnestock J.D., Schowengerdt R.A., "Spatially variant contrast enhancement using local range modification," *Optical Engineering*, vol. 22, pp. 378-381, 1983.

[FOLEY, 81] Foley W.D., Wilson C.R., Keyes G.S., et al., "The effects of varying spatial resolution on the detectability of diffuse pulmonary nodules," *Radiology*, vol. 141, pp. 25-31, 1981.

[FOLEY, 86] Foley W.D., Wilson C.R., San Dretto M., "The effect of varying high pass filter parameters on the detectability of diffuse pulmonary nodules," *Invest Radiol* , vol. 21, pp. 305-310, 1986.

[FOLEY, 87] Foley W.D., Goodman L.R., Wilson C., "Film digital radiography system: evaluation of interstitial lung disease," *Proceedings of the chest imaging conference*, Madison, WI, September 1987, pp. 96-109.

[FORREST, 82] Forrest J.V., Feigin D.S., "Essentials of Chest Radiology." : WB Saunders, 1982.

[FRASER, 83] Fraser R.G., Breatnach E., Barnes G.T., "Digital radiography of the chest: clinical experience with a prototype chest unit," *Radiology*, vol. 148, pp. 1-5, 1983.

[FREI, 77] Frei W., "Image enhancement by histogram hyperbolization," *Computer Graphics and Image Processing*, vol. 6, pp. 286-294, 1977.

[GOLDBERG, 89] Goldberg M., Robertson J., Belanger G., Georganas N., Mastronardi J., Cohn-sfetcu S., Dillon R., Tombaugh J., " A multimedia medical communication link between a radiology department and an emergency department," *SPIE Conference on Medical Imaging III*, Newport Beach, 1989.

[GONZALES, 77] Gonzales R.C., Fittes B.A., "Gray level transformations for interactive image enhancement," *Mechanism and machine theory* Pergamon Press,Great Britain, vol. 12, pp. 111-122, 1977.

[GOODMAN, 86] Goodman L.R., Foley W.D., Wilson C.R., et al., "Digital and conventional chest images: observer performance with film digital radiography system," *Radiology*, vol. 158, pp. 35-39, 1986.

[GOODMAN, 88] Goodman L.R., Foley W.D., Wilson C.R., Tikofsky RS., Hoffmann R.G., "Pneumothorax and other lung diseases: effect of altered resolution and edge enhancement on diagnosis with digitized radiographs," *Radiology*, vol. 167, pp. 83-88, 1988.

[GOODMAN, 88A] Goodman L.R., Wilson C.R., Foley W.D., "Digital radiography of the chest: promises and problems" *AJR*, vol. 150, pp. 1241-1252, 1988.

[HALL, 79] Hall E.l., *Computer Image Processing and Recognition*. New York:Academic Press, 1979.

[HEDGE, 86] Hedge SS. et al., "AT&T PACS Architecture", *Picture Archiving and Communication Systems (PACS IV) for Medical Applications*, pp. 818-625, 1986.

[HUANG, 87] Huang H.K., *Elements of Digital Radiology*. Englewood Cliffs, N.J.:Prentice Hall, 1987.

[HUMMEL, 77] Hummel R.A., "Image enhancement by histogram transformation," *Computer Graphics and Image Processing*, vol. 6, pp. 184-195, 1977.

[JACKSON, 82] Jackson P.H., Kaye G., "Chest radiograph enhancement using the weighted unsharp mask," *IBM UK Scientific Centre*, 1982.

[JOHNSON, 71] Johnson N.L., Kotz S., *Distributions in Statistics Continuous Univariate Distributions* 2. New York:John Wiley, 1971.

[JOHNSON, 83] Johnson G.A., Ravin C.E., "A survey of digital chest radiography," *Radiol. Clin. North Amer.*, vol. 21, pp. 655-665, 1983.

[JOHNSON, 85] Johnson G.A., Danieley N., Ravin C.E., "Processing alternatives for digital chest imaging," *Radiol. Clin. North Am.*, vol. 23, pp. 335-340, 1985.

[KETCHMAN, 76] Ketchman D.J., Lowe R.W., Weber J.W., "Real time image enhancement techniques" *Seminar on Image Processing*, Hugues Aircraft Pacific Grove, California, 1976, pp. 1-6.

[MASTRONARDI, 89] Mastronardi J., Beeton C., Reed S., Goldberg M., Robertson J., " Design of a Multimedia Communcation System for Clinical Trials at the Ottawa Civic Hospital," *SPIE Conference on Medical Imaging III*, Newport Beach, 1989.

[MCADAMS, 86] McAdams H.P., Johnson G.A., Suddarth A., Ravin C.E., "Histogram directed processing of digital chest images," *Invest. Radiol.*, vol. 21(3), pp. 233-253, 1986.

[MCADAMS, 87] McAdams P.A., Johnson A.G., Suddarth S.A., Sherrier R.H., Ravin C.E., "Implementation of adaptive filtration for digital chest imaging," *Optical Engineering*, vol. 26, no. 7, July 1987.

[MCLOUD, 84] McLoud T.C. "Digital chest radiography," *Proc. of the meeting of the Society of Thoracic Radiology*, pp. 186-187, 1984.

[MACMAHON, 85] MacMahon H., Vyborny C.J., Sabeti V., Doi K., Metz C.E., "The effect of digital unsharp masking on the detectability of interstitial infiltrates and pneumothoraces," *Proc. SPIE* , vol. 555, pp. 246-251, 1985.

[MACMAHON, 86] MacMahon H., Vyborny C.J., Metz C.E., Doi K., Sabeti V., Solomom S.L., "Digital radiography of subtle pulmonary abnormalities: an ROC of the effect of pixel size on observer performance," *Radiology* , vol. 158, pp. 21-26, 1986.

[MERRIT, 85] Merrit C.R., Matthews C.C. Scheinborn D., Balter S., "Digital imaging of the chest," *J. Thorac. Imag.*, vol. 1, pp. 1-13, 1985.

[NODINE, 87] Nodine C.F., Kundel H.L., "Using eye movements to study visual search and to improve tumor detection," *Radiographics*, vol. 7(6), pp. 1241-1250, 1987.

[NOSIL, 88] Nosil J. et al. "A prototype multi-modality picture and communication system at Victoria General Hospital," *Medical Imaging II: Image Data Management and Display*, 1988, vol. 914(B), pp. 1363-1378

[OGORMAN, 85] O'Gorman L. et al., "Entropy constant image enhancement by histogram transformation," *SPIE Applications of Digital Imaging VIII*, vol. 575, pp. 106-113, 1985.

[PIZER, 81] Pizer S.M., "Intensity mappings for the display of medical images," *Functional Mapping of Organ Systems and other Computer Topics* Society of Nuclear Medicine, pp. 205-217, 1981.

[PIZER, 87] Pizer S.M., Amburn E.P., Austin J.D., Cromartie R., et al., "Adaptive histogram equalization and its variations," *Computer Vision, Graphics and Image Processing*, vol. 39, pp. 355-368, 1987.

[PIZER, 87A] Pizer S.M., Johnston R.E., Rogers D.C., Beard D.V., "Effective presentation of medical images on an electronic display station," *Radiographics*, vol. 7(6), pp.1267-1274, 1987.

[PLESSIS, 89] Plessis B., Goldberg M., Dillon R., Tombaugh J., Robertson J., Belanger G., Hickey N., "Context-dependent enhancement for radiological images" *SPIE on Medical Imaging III*, Newport Beach, 1989.

[PRATT, 78] Pratt W.K., *Digital Image Processing*. New York:Wiley & Sons, 1978.

[RAVIN, 83] Ravin C.E., Johnson G.A., "The optimal chest radiograph," *Seminars in Respiratory Medicine*, vol. 5(1), pp. 1-14, 1983.

[SCHWARTZ, 77] Schwartz A.A., Soha J.M., "Variable Threshold Zonal Filtering", *Appl. Opt.*, vol. 16, pp. 1779-1781, 1977.

[SEELEY, 87] Seeley G.W., Fisher H.D., Stempski M.O., Borgstrom M., Bjelland J., Capp M.P., "Total Digital Radiology Department: Spatial Resolution Requirements," *AJR*, vol. 148, pp. 421-426, 1987.

[SHERRIER, 87] Sherrier R.H., Johnson G.A., "Regionally adaptive histogram equalization of the chest," *IEEE Trans. Med. Imaging*, vol. MI-6, pp. 1-7, 1987.

[SHERRIER, 88] Sherrier R.H., Chiles C., Wilkinson W.E., Johnson G.A., Ravin C.E., "Effects of image processing on nodule detection rates in digitized chest radiographs: ROC study of observer performance," *Radiology*, vol. 166, pp. 447-450, 1988.

[SKLANSKY, 78] Sklansky J., "Medical radiographic image processing and pattern recognition," *Proc. Int. Conf. Patt. Recogn. Image Processing*, 1978.

[SMATHERS, 85] Smathers R.L., Brody W.R., "Digital radiography: current and future trends," *Br. J. Radiol.*, vol. 58, pp. 285-307, 1985.

[SOMMER, 85] Sommer F.G., Smathers R.L., Wheat R.L., Alvarez R.E., Brody W.R., Cassel D.M., "Digital processing of films radiographs," *AJR*, vol. 144, pp. 191-196, 1985.

[TESIC, 83] Tesic M.M., Mattson R.A., Barnes G.T., Sones R.A., Stickney J.B., "Digital radiography of the chest: design features and considerations for a prototype unit," *Radiology*, vol. 148, pp. 259-264, 1983.

[TITTERINGTON, 85] Titterington D., Smith A., Makov U., *Statistical Analysis of Finite Mixture Distributions*. New York:Wiley & Sons, 1985.

[TUBBS, 87] Tubbs J.D., "A note on parametric image enhancement," *Pattern Recognition*, vol.20(6), pp. 617-621, 1987.

[VOSSEPOEL, 88] Vossepoel A., Stoel B.C., Meershock A.P., "Adaptive Histogram Equalization Using Variable Regions," *IEEE Medical Imaging*, pp. 351-353, 1988.

[WANG, 83] Wang D.C., Vagnucci A.H., Li C.C., "Digital image enhancement: a survey," *Comput. Vision Graphics Image Process*, vol. 24, pp. 363-381, 1983.